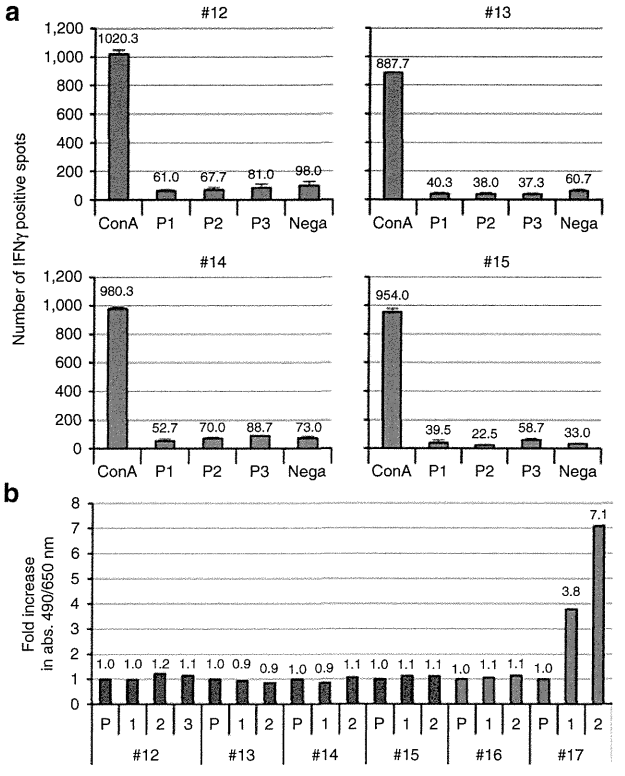

Figure 4 Detection of MazF-specific cellular and humoral immune responses. (a) IFN-γ enzyme-linked immunospot assay. The number of IFN-γ positive spots was measured under each stimulation condition. The PBMCs were prepared two months after the final MazF-Tmac cell transplantation. ConA: PBMCs from a MazF-Tmac-transplanted rhesus macaque were stimulated with concanavalin A. P1-3, PBMCs from a MazF-Tmac-transplanted rhesus macaque were stimulated with MazF peptide pools 1-3. Nega, nonstimulated PBMCs. Error bars represent the mean + SD. **(b)** Detection of MazF or ZsGreen1 specific humoral immune response using an enzyme-linked immunosorbent assay (ELISA). Plasma samples taken before transplantation (P), 4 weeks after the first transplantation,(1) 4 weeks after the second transplantation,(2) and 4 weeks after the third transplantation(3) of gene-modified cells were tested for the presence of antibodies against MazF in rhesus macaques #12, #13, #14, and #15 and for ZsGreen1 rhesus macaques #16 and #17. The relative fold increases in the absorbance values compared with the pretransplantation values are shown.

be used for surgical pathological analyses. We performed experimental autopsies at the end of the experiment. The histopathological findings of the specimens are summarized in **Supplementary Table S2**. Severe involution of the thymus was observed in rhesus macaque #12. This involution appeared to be the result of a physiological factor, such as aging, and was considered to be unrelated to the treatment of transplantation of MazF-Tmac cells. No serious adverse events related to MazF-Tmac cell transplantation were observed in any of the rhesus macaques in this treatment group.

Rhesus macaques #16 and #17 were affected by SHIV infection or transplantation of ZsG-Tmac cells, which have no SHIV resistance payload. As shown in **Supplementary Figure S3**, several disorders were observed in the axillary lymph nodes of the ZsG-Tmac-transplanted macaques,

Table 3 Distribution of gene-modified cells in lymphoid tissues

	MazF-Tmac transplantation							
	#12		#13		#14		#15	
	FCM (%)[a]	qPCR[b]	FCM (%)[a]	qPCR[b]	FCM (%)[a]	qPCR[b]	FCM (%)[a]	qPCR[b]
PBMC	4.1	2.9	15.4	18.0	4.8	11.1	11.8	26.4
Inguinal LN	N/A	3.0	13.2	16.8	4.2	8.1	7.3	17.1
Axillary LN	N/A	3.1	11.9	17.7	2.7	6.5	6.7	17.3
Mesenteric LN	N/A	0.54	13.0	18.2	4.0	10.1	5.6	14.3
Spleen	N/A	0.28	13.3	7.4	2.7	3.9	7.2	14.7

The lymphocytes isolated from several organs at autopsy were analyzed by flow cytometry and qPCR to determine the distribution of gene-modified cells.
FCM, flow cytometry; LN, lymph nodes; N/A, not applicable; PBMC, peripheral blood mononuclear cell.
[a]The percentage of ΔLNGFR-positive $CD4^+$ T cells was determined by flow cytometry. qPCR. [b]Proviral vector copy numbers per 10^2 $CD4^+$ T cells.

including a decrease in size, destruction of the structures, (see **Supplementary Figure S3a**) and a decrease in lymphoid cells (see **Supplementary Figure S3b**). These disorders were not observed in the MazF-Tmac-transplanted rhesus macaques. Rhesus macaque #16 was seriously affected by atrophy of the thymus, a decrease in lymphocytes in the inguinal and mesenteric lymph nodes, atrophy and lymphoid necrosis in the splenic marginal zone and a decrease in lymphoid cells in the periarterial lymphatic sheath and red pulp (see **Supplementary Table S2**). These observations were considered to be representative of changes relevant to the SHIV infection or transplantation of ZsG-Tmac cells. In rhesus macaque #17, atrophy of the thymus and a decrease in the lymphocytes in the inguinal lymph nodes were considered to be related to SHIV infection or the transplantation of ZsG-Tmac cells.

Function of persisting MazF-Tmac cells

To examine the Tat-dependent expression of MazF and its antiviral efficacy maintained in the rhesus macaques, $CD4^+$ T cells were isolated from the peripheral blood at 5 and 18 months after the first transplantation in rhesus macaques #13 and #15 and rhesus macaque #14, respectively. The expression of the MazF protein, the proviral copy numbers of SHIV and the production of SHIV in *ex vivo* culture were analyzed (Figure 5a).

A qPCR assay and Western blotting analysis were employed in PBMCs and isolated $CD4^+$ T cell samples from rhesus macaques #13 and #15 to detect the intact expression of MazF *in vivo*; however, there was no signal with either method. We speculate that the specific detection of MazF expression *in vivo* is challenging due to a limited number of MazF-Tmac cells in PBMCs and the low infectivity of SHIV *in vivo* compared with *in vitro* conditions. Next, the isolated $CD4^+$ T cells were expanded *ex vivo* for seven days, during which SHIV actively replicated, and Tat-dependent expression was expected to be induced in the MazF-Tmac cells in the $CD4^+$ T-cell population. The expression of MazF was observed in the expanded cells by Western blotting analysis (Figure 5b). Although the intact expression of MazF *in vivo* was below the detection limit by qPCR and Western blotting, the Tat-dependent conditional expression system was maintained long term after transplantation.

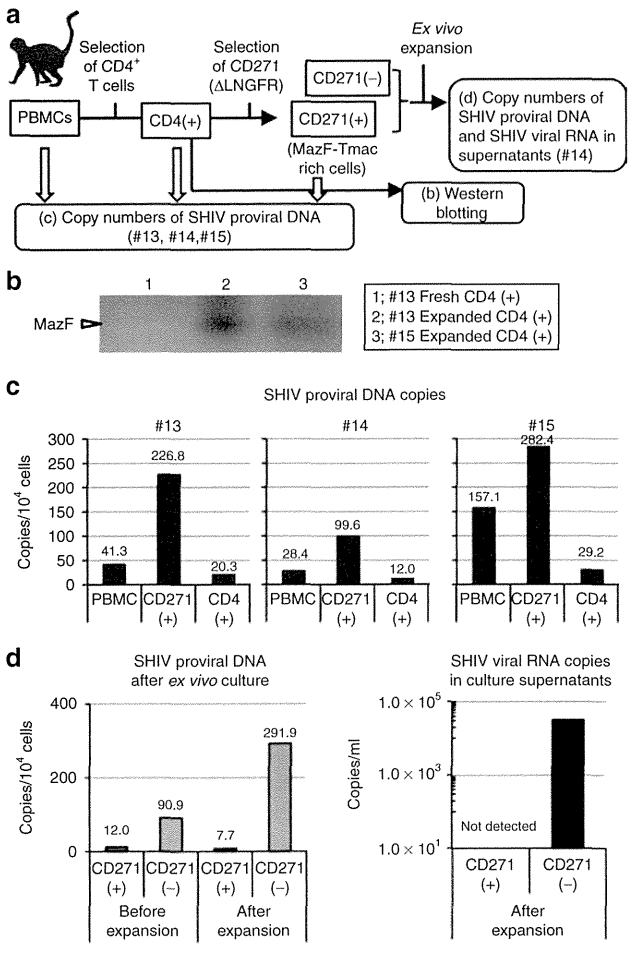

Figure 5 Function of long-term persisting MazF-Tmac cells. **(a)** Outline of the experiment. **(b)** CD4+ T cells were isolated from the peripheral blood of MazF-Tmac-transplanted rhesus macaques five months after the first transplantation. The isolated CD4+ T cells were expanded for seven days *ex vivo* and used for Western blotting analysis to detect the expression of MazF. **(c)** The CD271-positive and -negative cells were separated from the isolated CD4+ T cells of rhesus macaques #13, #14, and #15. DNA samples were collected from the PBMCs, the CD4+ T cells and the CD271+-MazF-Tmac-enriched population to analyze the proviral copy number of SHIV. **(d)** The CD271+-MazF-Tmac-enriched and CD271−-MazF-Tmac-negative populations isolated from rhesus macaque #14 were expanded *ex vivo* for 7 days. Changes in the SHIV proviral DNA levels in the cells and the SHIV RNA levels in the supernatants were analyzed in the CD271+-MazF-Tmac-enriched and CD271−MazF–Tmac-negative populations.

The persisted MazF-Tmac cells, which expressed the surface marker ΔLNGFR, were concentrated from a blood sample taken from rhesus macaques #13, #14, and #15 using an anti-CD271 monoclonal antibody. The number of proviral DNA copies of SHIV was measured in the PBMC population, CD4+ T-cell population and CD271+-MazF-Tmac-enriched population. As shown in Figure 5c, the number of proviral SHIV copies in the CD271+-MazF-Tmac-enriched population was one log lower than that in the CD4+ T-cell population in all three MazF-Tmac-transplanted rhesus macaques. To assess the function of the MazF-Tmac cells after transplantation, the CD271+-MazF-Tmac-enriched population and CD271−-MazF-Tmac-negative population isolated from rhesus macaque #14 at 18 months after transplantation were expanded *ex vivo* for 7 days in the absence of antiviral drugs. Changes in the SHIV proviral DNA level in the cells and the SHIV RNA level in the supernatants were analyzed. As shown in Figure 5d, the SHIV proviral DNA of the CD271−-MazF-Tmac-negative population increased by more than threefold after the expansion, indicating that SHIV was replicated in the CD271−-MazF-Tmac-negative population. The SHIV proviral DNA of the CD271+-MazF-Tmac-enriched population decreased slightly, indicating that replication of SHIV *ex vivo* was suppressed in the CD271+-MazF-Tmac-enriched population. The SHIV RNA copies accumulated in the supernatant of the CD271−-MazF-T-negative population in the absence of antiviral drugs, while there were no detectable SHIV RNA copies in the culture supernatants of the CD271+-MazF-Tmac-enriched population. These data indicate that the MazF-Tmac cells (CD271+ cells) are functional and possess the capability to suppress SHIV replication even one and a half years after transplantation.

Discussion

MazF is an endoribonuclease that specifically cleaves ACA sequences in RNA.[29] Because there are more than 240 ACA sequences in HIV-1 RNA, HIV-1 should have almost no chance to gain a MazF-related escape mutation. Therefore, anti-HIV-1 gene therapy using MazF is an attractive strategy to suppress a broad spectrum of HIV-1. HIV-1 Tat-dependent conditional expression of MazF in CD4+ T cells suppresses the replication of HIV-1 and SHIV 89.6P without affecting cellular mRNAs.[21,23] Because MazF is a bacterial protein and has never been tested in humans, it is important to assess the safety of the MazF-system *in vivo* using a nonhuman primate model. In a previous report, we showed the long-term persistence and safety of autologous transplantation of MazF-Tmac cells using cynomolgus macaques[25] that were not infected with a pathogenic virus. To obtain a better understanding of the MazF-modified CD4+ T cells in the presence of a viral infection *in vivo*, rhesus macaques were infected with pathogenic SHIV 89.6P and transplanted with autologous MazF-Tmac cells.

An engraftment of 1–2% of gene-modified cells in the peripheral circulation has been reported after the transplantation of approximately 10^{10} cells in adoptive T cell transfer gene therapy for humans,[13] and higher cell doses result in higher measurable engraftment levels.[30] We decided to transplant more than 10^9 cells in the primate model, reflecting one-tenth of the scale of the human gene therapy trials. To investigate the influence of repeated transplantations, transplantations were performed two or three times in this study.

The CD4+ T cell count values of the SHIV-infected rhesus macaques increased after the transplantation of the MazF-Tmac cells with statistical significance, while such increases were not observed in the ZsG-Tmac-transplanted rhesus macaques. The infused MazF-Tmac cells persisted for a long period *in vivo*, with half-lives ranging between 7.7 and 58 days. It is also possible that some of the MazF-Tmac cells were vigorously infected by SHIV and killed. To gain a longer

therapeutic benefit from the infusion of gene-modified T cells, gene-modified T cells are expected to expand *in vivo*; however, MazF-Tmac cells did not preferentially expand *in vivo* in this experiment. We are currently addressing this issue and attempting to confer self-expansion capability on MazF-Tmac cells in the presence of viral infections.

The viral load of MazF-Tmac-infused macaques did not decrease dramatically. In general, the major roles of CD4+ helper T cell are activation and regulation of the immune system. The helper T cell does not directly affect the viral load or infected cells as like cytotoxic T-lymphocytes or antibodies, so we speculate that the dramatic decrease of SHIV viral load was not observed though CD4+ T cell counts increased.

We used six rhesus macaques, which were divided in two arms—four rhesus macaques for MazF-modified T cell-treated arm and two macaques for ZsGreen1-modified T cell-treated arm. Only one rhesus macaque in the MazF-modified T cell-treated arm was highly infected with SHIV; the other three were weakly infected. However, SHIV proviral DNA was detected in the PBMCs of all of the macaques, and SHIV reproduced in culture medium when collected PBMCs were expanded *ex vivo* (Figure 5). The primary purpose of this experiment was to confirm the safety and persistence of MazF-Tmac cells in the presence of SHIV infection; thus, we used not only high viral load macaque but also weakly infected macaques for this study. No immune responses related to MazF were observed, and half-lives were extended after the repeated transplantation. The evidence of longitudinal persistence of MazF-Tmac cells suggests that MazF-modified T cells are not highly immunogenic. Because MazF remains at a constant low level upon viral infection,[23] MazF-Tmac cells are unlikely to activate an immune response. To obtain more safety information on MazF-modified CD4+ T cells in the presence of HIV infection, further investigations are needed, and a clinical trial entitled "A phase I, open label, dual cohort, single center study to evaluate the safety, tolerability and immunogenicity of autologous CD4 T cells modified with a retroviral vector expressing the *mazF* endoribonuclease gene in patients with HIV" is now ongoing in the United States (clinicaltrials.gov, identifier NCT01787994). Antiviral effect would also be assessed in the cohort 2 arm of this clinical trial.

In contrast, the infused ZsG-Tmac cells did not persist for an extended period *in vivo*, and the half-lives were not extended after repeated transplantation. The transient rebound of SHIV and marked decrease in the number of vector copies occurred simultaneously within 2 weeks after the transplantation of ZsG-Tmac cells; antiZsGreen1 antibodies developed gradually and reached their maximum level 40 days after the transplantation (see **Supplementary Figure S4**). We hypothesize that the ZsG-Tmac cells, which have no payload related to SHIV resistance, secreted a large amount of SHIV particles after infection and were destroyed by SHIV *in vivo*. The internalization of ZsGreen1 protein and antigen presentation by antigen-presenting cells induced the immune responses. In the case of rhesus macaque #17, ZsGreen1 protein might have been highly expressed by vigorous infection and triggered antibody production. In the case of rhesus macaque #16, ZsGreen1 protein was most likely expressed abundantly as in #17. Because this rhesus macaque exhibited severely reduced CD4+ T cell counts, we speculate that the B cells were not stimulated by Th2 effector cells due to a lack of CD4+ helper T cells; thus, no antibodies against ZsGreen1 were detected in rhesus macaque #16.

To address whether MazF-modified CD4+ T cells are associated with carcinogenicity *in vivo,* clonal expansion of the gene-modified cells was assessed using the linear amplification-mediated-PCR (LAM-PCR) method,[31] which traces the progeny of transduced cells by detecting the random insertion of the retrovirus or lentivirus vector. Although the preliminary data were collected from four macaques during a limited experimental period, there were no specific clonal expansions in any of the MazF-Tmac-transplanted rhesus macaques (see **Supplementary Figure S5**).

The histopathological analyses of the major organs, as well as the secondary lymphoid tissues, revealed that the transplantation of the MazF-Tmac cells was not associated with any carcinogenicity during the study period (see **Supplementary Figure S3** and **Supplementary Table S2**). A decrease in lymphocyte number was observed in the inguinal and axillary lymph nodes of the ZsG-Tmac-transplanted rhesus macaques (see **Supplementary Figure S3** and **Supplementary Table S2**). Although the transplanted ZsG-Tmac cells were not detected at the time of autopsy, the ZsG-Tmac cells might have migrated to the lymph nodes after transplantation, and the SHIV might have vigorously replicated in the migrated ZsG-Tmac cells, leading to cell death and, ultimately, bystander apoptosis of the neighboring uninfected cells and damage to the lymph nodes.[32] There was no such damage to the lymph nodes in rhesus macaque #12, which exhibited the highest SHIV viral loads and had undergone transplantation of MazF-Tmac cells three times.

Because gene therapy for HIV-1 should aim to reconstitute an HIV-1-resistant immune system, it is important for the gene-modified cells to not only inhibit viral replication but also maintain their distribution for long periods *in vivo*. Although the long-term persistence of gene-modified T cells or hematopoietic stem cells has been reported in the context of human gene therapy, it is difficult to obtain information about the distribution of these cells throughout the body. The use of primate models is advantageous for investigating the distribution pattern. At the time of the experimental autopsy, lymphocytes were isolated from the principal organs. MazF-Tmac cells were detected in the secondary lymphoid tissues, including several lymph nodes and the spleen, as well as the peripheral blood. A similar tendency was observed in previous data from cynomolgus macaques.[25] In contrast, ZsG-Tmac cells were not detected in any of the organs at the time of autopsy. The MazF-Tmac cells tend to persist primarily in the peripheral blood and secondary lymphoid tissues, regardless of the SHIV infection status.

The number of proviral SHIV DNA copies in the harvested CD271+-MazF-Tmac-enriched population was significantly lower than that in the CD4+ T-cell population (Figure 5c). The exact mechanism of low SHIV copies in MazF-Tmac cells *in vivo* remains unclear. We examined the expression of coreceptor CXCR4 in gene-modified cells at the time of infusion, and no difference in expression levels was observed between the gene-modified and unmodified cells. One possible hypothesis is that the majority of the SHIV-infected CD4+

T cells were infected at the acute infection stage but that the infused cells are less infected during chronic infection stage. Alternatively, leaky expression of MazF in the infused MazF-Tmac cells may inhibit the integration of SHIV. Another possibility is that vigorously infected MazF-Tmac cells died off after the over-induction of MazF expression. Further investigation is needed to reveal the mechanism.

We analyzed the function of the MazF-Tmac cells that persisted long after transplantation. Conditional MazF expression system was maintained and MazF protein expressed in T cells harvested from the rhesus macaques long after transplantation. In the freshly isolated samples, which are not expanded *ex vivo*, MazF signal was beyond detection (Figure 5b, lane 1). This phenomenon was considered due to low frequency of SHIV infection in MazF-Tmac cells (Figure 5c). However, we believe that low sensitivity to SHIV and low expression of MazF may contribute to the stable long-term persistence of MazF-Tmac cells, even in the presence of SHIV. Moreover, our qPCR analysis demonstrated that SHIV replication was blocked (Figure 5d). Although these data are from only one macaque, it appears that the MazF expression system was maintained, and the expressed MazF was functional long after transplantation.

Transplantation with MazF-Tmac cells contributed to an increase in the CD4$^+$ T cell counts, and the MazF-Tmac cells showed little or no immunogenicity in rhesus macaques in the presence of SHIV infection, suggesting that the autologous transplantation of MazF-modified CD4$^+$ T cells is an attractive strategy for HIV-1 gene therapy.

Materials and methods

General laboratory statement. Research sample processing and freezing were performed in a biosafety level (BSL) 3 laboratory at the Tsukuba Primate Research Center in the National Institute of Biomedical Innovation (NIBIO, Ibaraki, Japan). Laboratory analyses were performed in BSL2 laboratories at the Tsukuba Primate Research Center in NIBIO and at the Center for Cell and Gene Therapy of Takara Bio, which uses established standard operating procedures and protocols for sample processing, freezing, and analysis.

Study design. The animal study protocol was approved by the Ministry of Education, Culture, Sports, Science and Technology of Japan (identifier 20–8156), and by the Animal Welfare and Animal Care Committee of the NIBIO (identifier DS20-98R3). The study was conducted according to the "Rules for Animal Care and the Guiding Principles for Animal Experiments Using Nonhuman Primates" formulated by the Primate Society of Japan,[33] and in accordance with the recommendations of the Weatherall report, "The use of nonhuman primates in research" and the "Rules for Animal Care and Management of the Tsukuba Primate Research Center."[34] The experimental design is diagrammed in Figure 1. Six rhesus macaques, #12, #13, #14, #15, #16, and #17, were used for this experiment. CD4$^+$ T cells were isolated from the blood samples taken from each rhesus macaque before the challenge with SHIV and cryopreserved as described below. After confirming the set point of the SHIV viral loads, the gene-modified CD4$^+$ T cells were manufactured and transplanted as described in **Supplementary Materials**. Autologous CD4$^+$ T cells were transduced with the MazF retroviral vector MT-MFR-PL2 (#12, #13, #14, and #15) or the control vector MT-ZGR-PL2 (#16 and #17).

Animals. The Burmese rhesus macaques were maintained at the Tsukuba Primate Research Center in NIBIO. All surgical and invasive clinical procedures were conducted in a surgical facility using aseptic techniques and comprehensive physiologic monitoring. Ketamine hydrochloride (Ketalar, 10 mg/kg; Daiichi-Sankyo, Tokyo, Japan) was used to induce anesthesia for all clinical procedures associated with the study protocol, including blood sampling, gene-modified cell administration and clinical examinations or treatment.

SHIV 89.6P virus. A CXCR4-tropic SHIV 89.6P[26] was used for this experiment. SHIV 89.6P was propagated in rhesus macaque PBMCs. The culture supernatants were harvested, and the 50% tissue culture infective dose ($TCID_{50}$) was determined by infecting the CD4$^+$ human T-lymphoblastoid cell line M8166 with dilutions of the virus.[35] All the stock viruses were stored at −80°C until use. An intravenous challenge with SHIV 89.6P was performed at 5.0×10^3–1.8×10^5 $TCID_{50}$ (**Supplementary Table S1**).

Gibbon ape leukemia virus (GaLV)-enveloped gamma-retroviral vector MT-MFR-PL2 and MT-ZGR-PL2. The preparation of the retroviral vector used in this study has been previously described.[21] Briefly, an HIV-1-LTR-MazF-polyA cassette was introduced in the direction opposite of the MoMLV-LTR at the multiple cloning site of the retroviral vector plasmid pMT.[36] The Δ*LNGFR* gene[37] was introduced into the retrovirus vector as a surface marker. The Δ*LNGFR* gene is under the control of the human phosphoglycerate kinase (PGK) promoter. The resultant MT-MFR-PL2 was introduced into the packaging cell line PG13 (ATCC CRL-10686) and the GaLV-enveloped gamma-retroviral vector MT-MFR-PL2 was obtained by harvesting the culture fluid of the producer cells. For the control experiment, the *mazF* gene was replaced with the gene encoding the fluorescent ZsGreen1 protein (MT-ZGR-PL2). The GaLV-enveloped MT-ZGR-PL2 was obtained by harvesting the culture fluid of the PG13 derived producer cells.

CD4$^+$ T cells. Prior to the challenge with SHIV 89.6P, the peripheral blood of rhesus macaques was collected by apheresis as described previously.[38] The CD4$^+$ T cells were positively isolated using anti-CD4 antibody conjugated magnetic beads (Dynal CD4 Positive Isolation Kit, Life Technologies, Carlsbad, CA) according to the manufacturer's instructions. The isolated CD4$^+$ T cells were cryopreserved and stored at −80°C until use.

Manufacturing autologous gene-modified CD4$^+$ T cells and transplantation into rhesus macaques. Refer to the **Supplementary Materials**.

Measurement of hematological data. Refer to the **Supplementary Materials.**

Flow cytometry analyses. Refer to the **Supplementary Materials.**

Quantification of gene-modified CD4+ T cells. Refer to the **Supplementary Materials.**

Analyses of the SHIV viral loads in plasma. Refer to the **Supplementary Materials.**

Detection of MazF antigen-specific IFN-γ secreting cells. Refer to the **Supplementary Materials.**

Detection of anti-MazF or anti-ZsGreen1 antibodies in rhesus macaque blood. Refer to the **Supplementary Materials.**

Collection of lymphocytes from several organs. Refer to the **Supplementary Materials.**

Examination of function and antiviral efficacy of persisting MazF-Tmac cells. Refer to the **Supplementary Materials.**

LAM-PCR. Refer to the **Supplementary Materials.**

Western blotting. Refer to the **Supplementary Materials.**

Supplementary material

Figure S1. Body weight and hematological data.
Figure S2. MazF peptides used for the IFN-γ enzyme-linked immunospot assay.
Figure S3. Histopathological analysis of axillary lymph nodes.
Figure S4. Changes in SHIV viral loads, ZsGreen1 proviral copy numbers and production of anti-ZsGreen1 antibodies of rhesus macaque #17.
Figure S5. Linear amplification-mediated (LAM)-PCR.
Table S1. Dose of SHIV 89.6P TCID50 used to infect each rhesus macaque and the time of transplantation of the gene-modified cells.
Table S2. Analysis of the in vivo safety (individual histopathological findings from the autopsy samples).
Materials and methods

Acknowledgments. The authors thank the staff of the Tsukuba Primate Research Center and Corporation for Production and Research of Laboratory Primates for their kind care and expert handling of the animals. The authors thank Keith A. Reimann of Harvard Medical School and Tomoyuki Miura of Kyoto University for providing the SHIV 89.6P. The authors thank the members of the Center for Cell and Gene Therapy of Takara Bio Inc., Koichi Inoue and Katsuyuki Dodo for their contributions and helpful advice, and Hiroshi Tsuda, Tomomi Sakuraba, and Mayumi Shimomura for technical support. The authors have no support or funding to report. The animal study was designed by Hideto Chono, Naoki Saito, Hiroaki Shibata, Naohide Ageyama, Yasuhiro Yasutomi and Junichi Mineno. Gene-modified T cells were manufactured by Naoki Saito and Hideto Chono. All surgical and invasive clinical procedures were conducted under the supervision of Naohide Ageyama. Blood samples were prepared by Hiroaki Shibata. The laboratory analyses were performed by Naoki Saito. The manuscript was written by Hideto Chono and Naoki Saito. All authors discussed and interpreted results. Naoki Saito, Hideto Chono and Junichi Mineno are employees of Takara Bio Inc. (http://www.takara-bio.com). European patent applications EP1921136B1 "Nucleic acid for treatment or prevention of immunodeficiency virus infection" and EP2138580B1 "Vector for gene therapy" were filed through Takara Bio Inc. These interests do not alter the authors' adherence to the Journal's policies regarding sharing data and materials. The other authors declared that they have no competing interests.

1. Kitahata, MM, Gange, SJ, Abraham, AG, Merriman, B, Saag, MS, Justice, AC *et al.* (2009). Effect of early versus deferred antiretroviral therapy for HIV on survival. *N Engl J Med* **360**: 1815–1826.
2. Maartens, G and Boulle, A (2007). CD4 T-cell responses to combination antiretroviral therapy. *Lancet* **370**: 366–368.
3. Geng, EH and Deeks, SG (2009). CD4+ T cell recovery with antiretroviral therapy: more than the sum of the parts. *Clin Infect Dis* **48**: 362–364.
4. Lekakis, J and Ikonomidis, I (2010). Cardiovascular complications of AIDS. *Curr Opin Crit Care* **16**: 408–412.
5. Núñez, M (2010). Clinical syndromes and consequences of antiretroviral-related hepatotoxicity. *Hepatology* **52**: 1143–1155.
6. Cheung, MC, Pantanowitz, L and Dezube, BJ (2005). AIDS-related malignancies: emerging challenges in the era of highly active antiretroviral therapy. *Oncologist* **10**: 412–426.
7. Siliciano, RF and Greene, WC (2011). HIV latency. *Cold Spring Harb Perspect Med* **1**: a007096.
8. Richman, DD, Margolis, DM, Delaney, M, Greene, WC, Hazuda, D and Pomerantz, RJ (2009). The challenge of finding a cure for HIV infection. *Science* **323**: 1304–1307.
9. Hütter, G, Nowak, D, Mossner, M, Ganepola, S, Müssig, A, Allers, K *et al.* (2009). Long-term control of HIV by CCR5 Delta32/Delta32 stem-cell transplantation. *N Engl J Med* **360**: 692–698.
10. Allers, K, Hutter, G, Hofmann, J, Loddenkemper, C, Rieger, K, Thiel, E *et al.* (2011). Evidence for the cure of HIV infection by CCR5Delta32/Delta32 stem cell transplantation. *Blood* **117**: 2791–2799.
11. Sarver, N and Rossi, J (1993). Gene therapy: a bold direction for HIV-1 treatment. *AIDS Res Hum Retroviruses* **9**: 483–487.
12. Dropulić, B and Jeang, KT (1994). Gene therapy for human immunodeficiency virus infection: genetic antiviral strategies and targets for intervention. *Hum Gene Ther* **5**: 927–939.
13. Levine, BL, Humeau, LM, Boyer, J, MacGregor, RR, Rebello, T, Lu, X *et al.* (2006). Gene transfer in humans using a conditionally replicating lentiviral vector. *Proc Natl Acad Sci USA* **103**: 17372–17377.
14. Morris, KV and Rossi, JJ (2006). Lentivirus-mediated RNA interference therapy for human immunodeficiency virus type 1 infection. *Hum Gene Ther* **17**: 479–486.
15. Rossi, JJ, June, CH and Kohn, DB (2007). Genetic therapies against HIV. *Nat Biotechnol* **25**: 1444–1454.
16. van Lunzen, J, Glaunsinger, T, Stahmer, I, von Baehr, V, Baum, C, Schilz, A *et al.* (2007). Transfer of autologous gene-modified T cells in HIV-infected patients with advanced immunodeficiency and drug-resistant virus. *Mol Ther* **15**: 1024–1033.
17. Li, MJ, Kim, J, Li, S, Zaia, J, Yee, JK, Anderson, J *et al.* (2005). Long-term inhibition of HIV-1 infection in primary hematopoietic cells by lentiviral vector delivery of a triple combination of anti-HIV shRNA, anti-CCR5 ribozyme, and a nucleolar-localizing TAR decoy. *Mol Ther* **12**: 900–909.
18. Hoxie, JA and June, CH (2012). Novel cell and gene therapies for HIV. *Cold Spring Harb Perspect Med* **2**: a007179.
19. Cannon, P and June, C (2011). Chemokine receptor 5 knockout strategies. *Curr Opin HIV AIDS* **6**: 74–79.
20. Tebas, P, Stein, D, Binder-Scholl, G, Mukherjee, R, Brady, T, Rebello, T *et al.* (2013). Antiviral effects of autologous CD4 T cells genetically modified with a conditionally replicating lentiviral vector expressing long antisense to HIV. *Blood* **121**: 1524–1533.
21. Chono, H, Matsumoto, K, Tsuda, H, Saito, N, Lee, K, Kim, S *et al.* (2011). Acquisition of HIV-1 resistance in T lymphocytes using an ACA-specific E. coli mRNA interferase. *Hum Gene Ther* **22**: 35–43.
22. Shimazu, T, Degenhardt, K, Nur-E-Kamal, A, Zhang, J, Yoshida, T, Zhang, Y *et al.* (2007). NBK/BIK antagonizes MCL-1 and BCL-XL and activates BAK-mediated apoptosis in response to protein synthesis inhibition. *Genes Dev* **21**: 929–941.
23. Okamoto, M, Chono, H, Kawano, Y, Saito, N, Tsuda, H, Inoue, K *et al.* (2013). Sustained inhibition of HIV-1 replication by conditional expression of the *E. coli*-derived endoribonuclease MazF in CD4+ T cells. *Hum Gene Ther Methods* **24**: 94–103.

24. Berkhout, B, Silverman, RH and Jeang, KT (1989). Tat trans-activates the human immunodeficiency virus through a nascent RNA target. *Cell* **59**: 273–282.
25. Chono, H, Saito, N, Tsuda, H, Shibata, H, Ageyama, N, Terao, K *et al.* (2011). *In vivo* safety and persistence of endoribonuclease gene-transduced CD4+ T cells in cynomolgus macaques for HIV-1 gene therapy model. *PLoS One* **6**: e23585.
26. Reimann, KA, Li, JT, Voss, G, Lekutis, C, Tenner-Racz, K, Racz, P *et al.* (1996). An env gene derived from a primary human immunodeficiency virus type 1 isolate confers high *in vivo* replicative capacity to a chimeric simian/human immunodeficiency virus in rhesus monkeys. *J Virol* **70**: 3198–3206.
27. Pitcher, CJ, Hagen, SI, Walker, JM, Lum, R, Mitchell, BL, Maino, VC *et al.* (2002). Development and homeostasis of T cell memory in rhesus macaque. *J Immunol* **168**: 29–43.
28. Klebanoff, CA, Gattinoni, L, Torabi-Parizi, P, Kerstann, K, Cardones, AR, Finkelstein, SE *et al.* (2005). Central memory self/tumor-reactive CD8+ T cells confer superior antitumor immunity compared with effector memory T cells. *Proc Natl Acad Sci USA* **102**: 9571–9576.
29. Zhang, Y, Zhang, J, Hoeflich, KP, Ikura, M, Qing, G and Inouye, M (2003). MazF cleaves cellular mRNAs specifically at ACA to block protein synthesis in *Escherichia coli*. *Mol Cell* **12**: 913–923.
30. Ranga, U, Woffendin, C, Verma, S, Xu, L, June, CH, Bishop, DK *et al.* (1998). Enhanced T cell engraftment after retroviral delivery of an antiviral gene in HIV-infected individuals. *Proc Natl Acad Sci USA* **95**: 1201–1206.
31. Schmidt, M, Zickler, P, Hoffmann, G, Haas, S, Wissler, M, Muessig, A *et al.* (2002). Polyclonal long-term repopulating stem cell clones in a primate model. *Blood* **100**: 2737–2743.
32. Ahr, B, Robert-Hebmann, V, Devaux, C and Biard-Piechaczyk, M (2004). Apoptosis of uninfected cells induced by HIV envelope glycoproteins. *Retrovirology* **1**: 12.
33. Primate Society of Japan (1986). Guiding principles for animal experiments using nonhuman primates. *Primate Res* **2**: 111–113.
34. Honjo, S (1985). The Japanese Tsukuba Primate Center for Medical Science (TPC): an outline. *J Med Primatol* **14**: 75–89.
35. Akiyama, H, Ido, E, Akahata, W, Kuwata, T, Miura, T and Hayami, M (2003). Construction and *in vivo* infection of a new simian/human immunodeficiency virus chimera containing the reverse transcriptase gene and the 3' half of the genomic region of human immunodeficiency virus type 1. *J Gen Virol* **84**(Pt 7): 1663–1669.
36. Lee, JT, Yu, SS, Han, E, Kim, S and Kim, S (2004). Engineering the splice acceptor for improved gene expression and viral titer in an MLV-based retroviral vector. *Gene Ther* **11**: 94–99.
37. Verzeletti, S, Bonini, C, Marktel, S, Nobili, N, Ciceri, F, Traversari, C *et al.* (1998). Herpes simplex virus thymidine kinase gene transfer for controlled graft-versus-host disease and graft-versus-leukemia: clinical follow-up and improved new vectors. *Hum Gene Ther* **9**: 2243–2251.
38. Ageyama, N, Kimikawa, M, Eguchi, K, Ono, F, Shibata, H, Yoshikawa, Y *et al.* (2003). Modification of the leukapheresis procedure for use in rhesus monkeys (Macaca mulata). *J Clin Apher* **18**: 26–31.

Supplementary Information accompanies this paper on the Molecular Therapy–Nucleic Acids website (http://www.nature.com/mtna)

OPEN

Nanogel-based pneumococcal surface protein A nasal vaccine induces microRNA-associated Th17 cell responses with neutralizing antibodies against *Streptococcus pneumoniae* in macaques

Y Fukuyama[1], Y Yuki[1,2], Y Katakai[3], N Harada[4], H Takahashi[5], S Takeda[5], M Mejima[1], S Joo[1], S Kurokawa[1], S Sawada[5], H Shibata[6], EJ Park[1], K Fujihashi[7], DE Briles[8], Y Yasutomi[6], H Tsukada[4], K Akiyoshi[5] and H Kiyono[1,2]

We previously established a nanosized nasal vaccine delivery system by using a cationic cholesteryl group-bearing pullulan nanogel (cCHP nanogel), which is a universal protein-based antigen-delivery vehicle for adjuvant-free nasal vaccination. In the present study, we examined the central nervous system safety and efficacy of nasal vaccination with our developed cCHP nanogel containing pneumococcal surface protein A (PspA-nanogel) against pneumococcal infection in nonhuman primates. When [^{18}F]-labeled PspA-nanogel was nasally administered to a rhesus macaque (*Macaca mulatta*), longer-term retention of PspA was noted in the nasal cavity when compared with administration of PspA alone. Of importance, no deposition of [^{18}F]-PspA was seen in the olfactory bulbs or brain. Nasal PspA-nanogel vaccination effectively induced PspA-specific serum IgG with protective activity and mucosal secretory IgA (SIgA) Ab responses in cynomolgus macaques (*Macaca fascicularis*). Nasal PspA-nanogel-induced immune responses were mediated through T-helper (Th) 2 and Th17 cytokine responses concomitantly with marked increases in the levels of miR-181a and miR-326 in the serum and respiratory tract tissues, respectively, of the macaques. These results demonstrate that nasal PspA-nanogel vaccination is a safe and effective strategy for the development of a nasal vaccine for the prevention of pneumonia in humans.

INTRODUCTION

Streptococcus pneumoniae is a major cause of bacterial infections throughout the world and is involved in the induction of a wide variety of infectious diseases, including otitis media, pneumonia, bacteremia, and meningitis in children and adults. This organism is usually a commensal bacterium in the upper respiratory tract of humans. Currently, four pneumococcal vaccines, 7-, 10- and 13-valent polysaccharide conjugate vaccines (PCV7, 10, 13) for children and a 23-valent pneumococcal polysaccharide vaccine (PPV23) for adults, have been developed for public use and are delivered by intramuscular injection.[1–3] However, as the conjugate vaccine does not protect against other capsular types, it provides little or no protection against total colonization with pneumococci.[4,5] The extensive carriage by other pneumococcal capsular types has led to strain replacement in disease with strains of non-conjugate vaccine capsular types.[6,7]

[1]Division of Mucosal Immunology, The Institute of Medical Science, The University of Tokyo, Minato-ku, Tokyo, Japan. [2]International Research and Development Center for Mucosal Vaccine, The Institute of Medical Science, The University of Tokyo, Minato-ku, Tokyo, Japan. [3]Corporation for Production and Research of Laboratory Primates, Tsukuba, Ibaraki, Japan. [4]PET Center, Central Research Laboratory, Hamamatsu Photonics K.K., Hamamatsu, Shizuoka, Japan. [5]Department of Polymer Chemistry, Kyoto University Graduate School of Engineering, Nishikyo-ku, Kyoto, Japan. [6]Tsukuba Primate Research Center, National Institute of Biomedical Innovation, Tsukuba, Ibaraki, Japan. [7]Departments of Pediatric Dentistry and Microbiology, The Immunobiology Vaccine Center, The University of Alabama at Birmingham, Birmingham, Alabama, USA and [8]Department of Microbiology, The University of Alabama at Birmingham, Birmingham, Alabama, USA. Correspondence: Y Yuki or H Kiyono (yukiy@ims.u-tokyo.ac.jp or kiyono@ims.u-tokyo.ac.jp)

Received 1 June 2014; accepted 2 January 2015; advance online publication 11 February 2015. doi:10.1038/mi.2015.5

The development of effective protein-based vaccines, which have the potential to provide better coverage for all strains, and to protect against colonization with all strains requires a thorough understanding of the roles and relative contributions to pathogenesis of the various putative virulence proteins. The pneumococcal surface protein A (PspA) is a well-known highly immunogenic surface protein of *S. pneumoniae* and is considered to be a promising vaccine candidate.[8,9] It is present on virtually all strains of pneumococci, and PspA-based vaccines against *S. pneumoniae* induce cross-reactive Abs in mice[10,11] and humans.[12] Moreover, PspA-specific mucosal and serum Abs responses are induced, and these responses are mediated by both Th1- and Th2-type cytokine production by $CD4^+$ T cells in infant mice via maternal immunization,[13] as well as in aged mice.[14] These findings indicate that PspA is a potent antigen for the development of effective pneumococcal vaccines not only in adults but also in children and the elderly.

S. pneumoniae commonly colonizes the nasal cavity, which can be protected by mucosal IgA.[15–17] Nasal vaccination induces effective mucosal immune responses in the respiratory tract, where initial bacterial and viral infections commonly occur; it could therefore be an effective immunization strategy for delivering protection from pneumococcal infection. However, most subunit type vaccines are poor immunogens for the induction of antigen-specific immune response in both systemic and mucosal immune compartments when nasally administered. Thus, the co-administration of biologically active mucosal adjuvants (e.g., cholera toxin and heat-labile toxin) or a better delivery system is needed to overcome the disadvantages of nasal antigen exposure. However, there are currently no safe nasal adjuvants or delivery systems, as evaluated by safety pharmacology studies, such as absorption, distribution, metabolism, and excretion in preclinical studies.

To overcome these concerns, we recently developed an effective vaccine delivery system with a self-assembled nanosized hydrogel (nanogel), which is composed of a cationic type of cholesteryl group-bearing pullulan (cCHP).[18] This cCHP nanogel efficiently delivers an antigen to epithelial cells in the nasal cavity, as well as to dendritic cells (DCs) under the basement membrane, and induces antigen-specific immune responses as an adjuvant-free vaccine.[19,20] Furthermore, a radioisotope counting assay showed that nasally administered cCHP nanogel carrying the [^{111}In]-labeled non-toxic subunit of botulinum neurotoxin does not accumulate in parts of the central nervous system (CNS) in mice.[19] In our separate study, we demonstrated that a nasally administered PspA-nanogel vaccine is safe and induces strong antigen-specific systemic and mucosal Ab immune responses, which can protect mice from invasive challenge with *S. pneumoniae*.[21]

MicroRNAs (miRNAs) have emerged as important regulators of many biological processes associated with the immune system, including the function of both innate and adaptive immune responses.[22–24] Accumulating evidence indicates that miRNA has an essential role in eliciting immune responses. For example, mice with T lymphocytes in which the endoribonuclease dicer, which is critical for miRNA biogenesis, has been conditionally knocked out show impaired thymic development and diminished Th-cell differentiation.[25,26] Dicer deficiency in B cells also prevents B-cell development.[27] These findings indicate the critical functions of miRNAs in the biology of the cells that constitute the immune system, such as in the development and differentiation of lymphocytes. Therefore, it is important to identify the miRNA biomarkers that engage in both mucosal and systemic antibody responses induced by nasal immunization with PspA-nanogel. Together, better understanding of the precise engagement of miRNAs in mediating humoral and protective immunity will be beneficial for the development of effective mucosal vaccines.

Before pursuing a clinical trial of a PspA-nanogel-based vaccine, we designed experiments to assess its safety for the CNS and its immunological efficacy, including immunologically relevant miRNA expression, and to demonstrate its safety and efficacy in nonhuman primates.

RESULTS

[^{18}F]-PspA-nanogel is retained for a long time in the nasal cavity but is not deposited in the olfactory bulbs or brain after nasal administration in macaques

We initially confirmed the physicochemical characterization of PspA-nanogel vaccine used in this study (**Supplementary Figure S1** online), and then investigated the retention of nasal PspA-nanogel in the nasal cavity and its accumulation in the olfactory bulbs and CNS in nonhuman primates by using three naive rhesus macaques. Because the results were nearly identical for the three macaques, we show the results for only one of the macaques in **Figure 1** (primate #1). The macaque's head was placed in the positron emission tomography (PET) scanner system and real-time imaging was performed for 6 h. To confirm the exact position of the cerebrum, we performed a magnetic resonance imaging (MRI) scan and then superimposed the PET images onto the MRI images. The real-time PET images clearly showed that nasally administered [^{18}F]-PspA-nanogel was effectively delivered to the nasal mucosa and retained in the nasal tissues for up to 6 h (**Figure 1a,c**). In contrast, most of the free form of [^{18}F]-PspA without a nanogel had disappeared from the nasal cavity by 3 h after nasal administration (**Figure 1a**). Furthermore, no deposition of [^{18}F]-PspA was detected in the cerebrum or olfactory bulbs of macaques, even 6 h after nasal administration (**Figure 1b**). These results show that PspA-nanogel is a CNS-safe and effective nasal vaccine delivery system in nonhuman primates.

Nasal vaccination with PspA-nanogel induces mucosal and systemic Ab responses in macaques

We next examined whether the nasal PspA-nanogel vaccine induced PspA-specific immune responses in cynomolgus macaques (primates #2-#9). One week after the final immunization, PspA-specific serum IgG Ab responses were significantly increased in macaques nasally immunized with 25 μg of PspA-nanogel when compared with macaques immunized with PspA alone or PBS only (**Figure 2a**). Examination of the longevity of PspA-nanogel-induced serum antigen-specific IgG

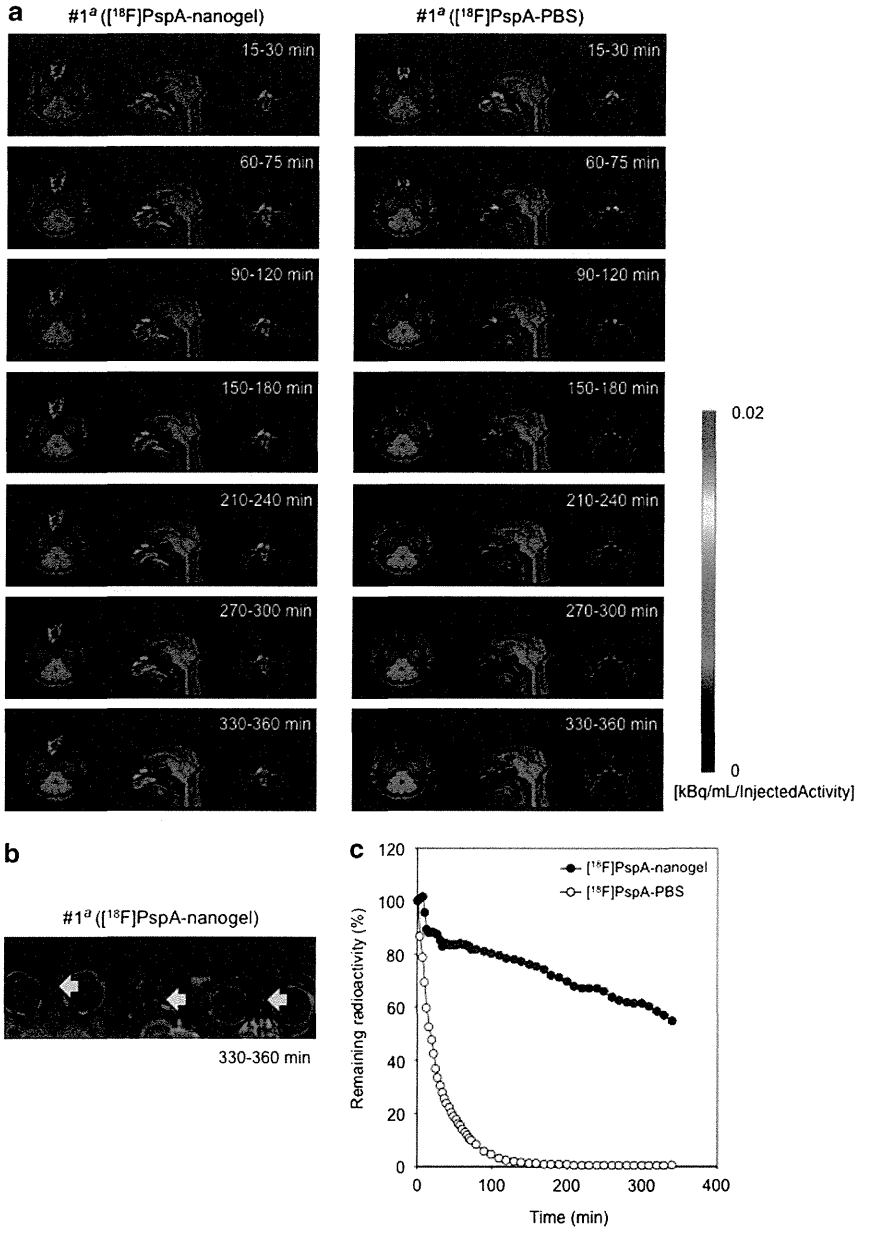

Figure 1 PET/MRI images (**a**,**b**) and TACs (**c**) for nasal administration of [^{18}F]-PspA-nanogel or [^{18}F]-PspA-PBS in a naive rhesus macaque. (**a**) After nasal administration of [^{18}F]-PspA-nanogel or [^{18}F]-PspA-PBS, the macaque's head was scanned for 6 h with a PET scanner. Real-time PET images overlaid on MRI images are shown for the indicated times post-administration. (**b**) To further check whether [^{18}F]-PspA accumulated in the CNS or olfactory bulbs (indicated by arrowheads), PET images taken at 6 h post-administration of [^{18}F]-PspA-nanogel were enlarged. (**c**) TACs for the nasal cavity for 6-h period after nasal administration of [^{18}F]-PspA-nanogel or [^{18}F]-PspA-PBS are presented. The data are expressed as percentages of the dose remaining after nasal administration. *a*: The same macaque was nasally administered of [^{18}F]-PspA-nanogel or [^{18}F]-PspA-PBS with a 1-week interval between administrations. CNS, central nervous system; MRI, magnetic resonance imaging; PET, positron emission tomography; TACs, time-activity curves.

Ab titers revealed that Ab levels gradually decreased over a period of 8 months in macaques nasally immunized with PspA-nanogel. Similarly, PspA-specific bronchoalveolar lavage fluid (BALF) IgG and nasal wash IgA Ab responses exhibited higher levels in macaques nasally immunized with PspA-nanogel when compared with macaques nasally immunized with PspA alone or PBS only (**Figure 2b,c**), and these Ab levels were also gradually decreased. In addition, PspA-specific BALF IgA Ab responses were slightly increased in two of the immunized macaques (#3 and #5) (**Figure 2c**).

When these macaques were given a dose of nasal booster of PspA-nanogel 9 months after the final immunization, the levels of PspA-specific serum and BALF IgG and nasal wash IgA Ab responses immediately recovered to those observed at 9 weeks

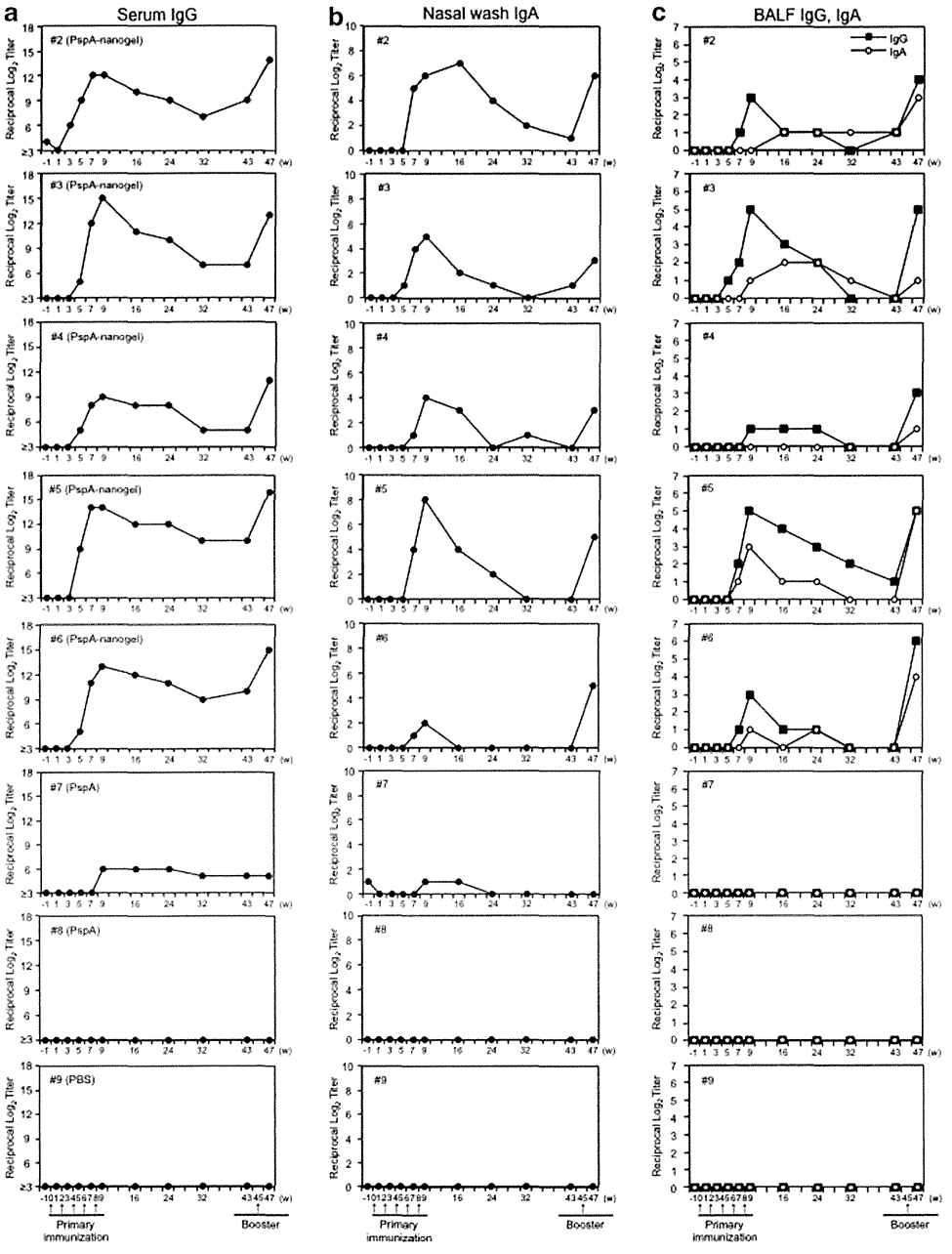

Figure 2 Nasal immunization with PspA-nanogel induced PspA-specific Ab responses in macaques. Each cynomolgus macaque was nasally immunized with PspA-nanogel (macaques #2-#6), PspA alone (#7 and #8), or PBS only (#9) at the times indicated with arrows. Serum, nasal wash, and BALF were collected, and the levels of PspA-specific serum IgG (**a**), nasal wash IgA (**b**), and BALF IgG and IgA (**c**) were determined by ELISA. BALF, bronchoalveolar lavage fluid.

after the initial PspA-nanogel immunization (**Figure 2a–c**). Of importance, a nasal booster induced higher levels of PspA-specific IgA Ab responses in BALF of two macaques (#5 and #6) than those observed after the primary immunization (**Figure 2c**).

These findings suggest that memory-type PspA-specific Ab responses are induced in nonhuman primates after nasal vaccination with PspA-nanogel. PspA-nanogel is therefore a promising nasal vaccine candidate that can induce long-lasting antigen-specific systemic and mucosal immunity and can elicit nasal booster activity in nonhuman primates.

Nasal immunization with PspA-nanogel induces neutralizing Abs against *S. pneumoniae* in macaques

To investigate whether the nasal PspA-nanogel vaccine induced neutralizing Abs, we examined whether PspA-specific serum Abs from macaques nasally immunized with PspA-nanogel would passively protect against pneumococcal infection. CBA/N mice were injected intraperitoneally with diluted pooled sera of macaques nasally immunized with PspA-nanogel, PspA alone, or PBS only. When all groups of mice were challenged with *S. pneumoniae* Xen10 or 3JYP2670 strain via the intravenous route, mice passively immunized with sera

from macaques nasally immunized with PspA-nanogel were fully protected for at least 2 weeks (**Figure 3a,b**). In contrast, mice that received sera from macaques given nasal PspA alone or PBS only died within 5 days post-challenge (**Figure 3a,b**). These results demonstrated that protective immunity with subtype cross-reactivity was induced by nasal PspA-nanogel vaccination.

Nasal immunization with PspA-nanogel induces Th2 and Th17 responses in macaques

As macaques nasally immunized with PspA-nanogel showed high IgG/IgA Ab responses, we next determined the levels of cytokine production in $CD4^+$ T cells isolated from blood of the macaques. The macaques nasally immunized with PspA-nanogel showed increased levels of IL-4 and IL-17 production by $CD4^+$ T cells when compared with macaques given PspA alone or PBS only (**Figure 4b,c**). However, essentially identical levels of IFN-γ were produced by $CD4^+$ T cells isolated from macaques nasally immunized with PspA-nanogel, PspA alone, or PBS only (**Figure 4a**). Furthermore, we showed that nasal immunization with PspA-nanogel induced PspA-specific IgG1 Ab responses, which is the hallmark of the Th2-type immune response (**Figure 4d**). These results indicated that the nasal PspA-nanogel vaccine could induce Th2 and Th17 cytokine responses.

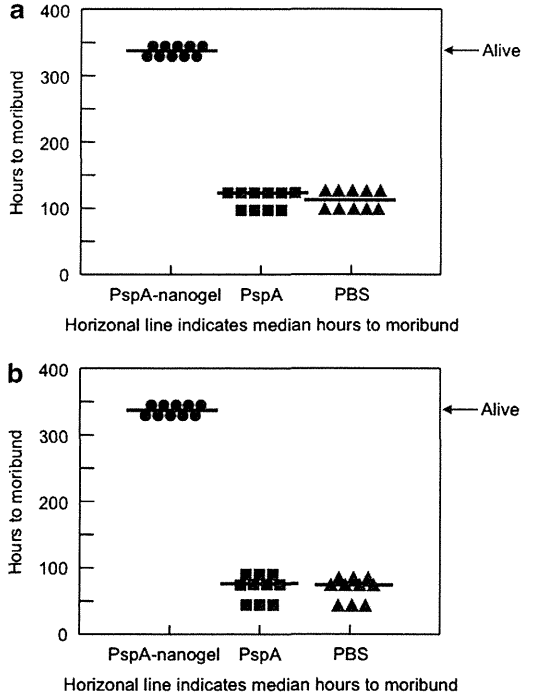

Figure 3 Neutralizing Abs induced by nasal immunization with PspA-nanogel. Serum from each of the macaques was collected 1 week after the final primary nasal immunization with PspA-nanogel, PspA alone, or PBS only. CBA/N mice (10 mice per group) were passively transferred with 100 μl of diluted (1:20) pooled sera via i.p. route. Four hours later, mice were injected i.v. with 1.5×10^4 c.f.u. *S. pneumoniae* Xen 10 (**a**) or 1×10^3 c.f.u. *S. pneumoniae* 3JYP2670 strain (**b**). The mice were monitored daily for mortality. Each line represents the median survival time. c.f.u., colony-forming unit; i.p., intraperitoneal; i.v., intravenous.

Nasal immunization with PspA-nanogel increases the expression levels of miRNAs in serum and respiratory tract tissues in macaques

To examine the roles of miRNA in the induction of PspA-specific immunity, we performed miRNA microarray analysis to identify immunologically associated differences in serum miRNA profiles between pre-immunized and post-boosted macaques (data not shown). We selected some immunologically relevant miRNAs, namely miR-181a, miR-326, miR-155, miR-17, miR-18a, miR-20a, and miR-92a, the levels of which were upregulated in post-booster serum samples compared with pre-immunized serum samples. To further confirm whether these immunologically relevant miRNAs were upregulated or downregulated in post-booster serum samples compared with pre-immunized or pre-booster serum samples, we performed quantitative RT–PCR of them. Expression levels of miR-326, Th17-cell differentiation-related miRNA, and miR-181a, T-cell and B-cell differentiation-related miRNA, were significantly increased in the sera of macaques given a nasal booster dose of PspA-nanogel when compared with control macaques as pre-immunization (**Figure 5a**). The levels of the two miRNAs were also shown significantly higher in the respiratory tract tissues, including nasal tissues and lungs, of macaques given a booster dose of PspA-nanogel than the levels in the corresponding tissues of control macaques given PspA alone or PBS only that was set at 1 (**Figure 5b,c**). Furthermore, we analyzed the expression level of Ets-1, which is a known negative regulator of Th17 cells and is the functional target of miR-326. We detected a significant decrease in the expression level of Ets-1 mRNA in the lungs of macaques given a booster dose of PspA-nanogel compared with those of control macaques given PspA alone or PBS only (**Figure 5c**). These results suggest that these miRNAs have important roles in T-cell and B-cell differentiation and in Th17 cytokine responses after nasal immunization with PspA-nanogel in macaques.

DISCUSSION

By using a nonhuman primate system, we demonstrated that the nasal PspA-nanogel vaccine did not accumulate in the CNS and effectively induced both mucosal and systemic immunity associated with protection against pneumococcal infection. To our knowledge, this study is the first to report the safety and effectiveness of a nasal PspA vaccine in macaques; therefore, our results provide a concrete rationale for testing our nanogel-based PspA vaccine in humans.

The nanogel itself is non-immunogenic material, and a cancer-specific protein (e.g., Her 2) complexed with a neutral CHP nanogel produced by means of good manufacturing practices (GMP) has been used as an injectable cancer vaccine in clinical research.[28] In our previous study, nasal immunization with CHP-nanogel containing PspA induces effective antigen-specific immune responses in mice[21] but not in macaques (data not shown); therefore, in the present study, we developed a cCHP nanogel containing 20 amino groups per 100 glucose units to improve antigen delivery to the nasal

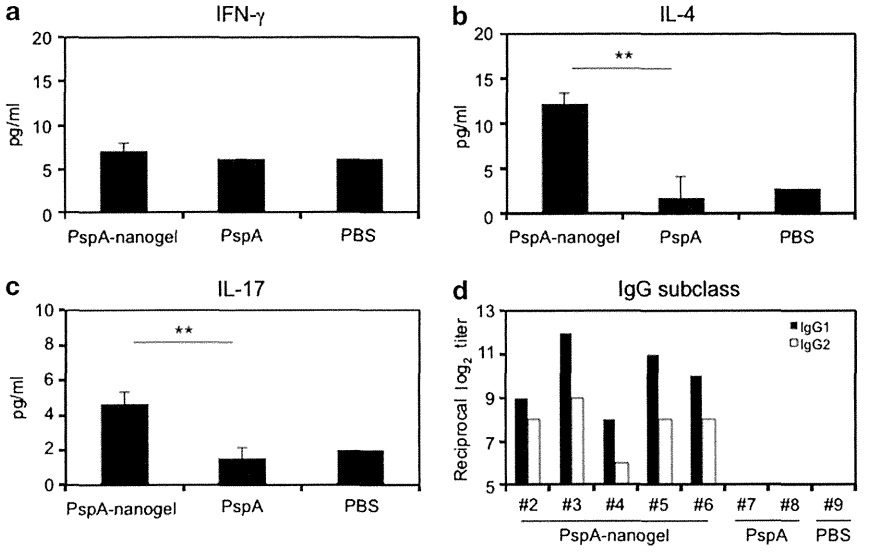

Figure 4 PspA-nanogel immunization produced CD4$^+$ Th2- and Th17-type cytokine responses. CD4$^+$ T cells were separated from the PBMCs 1 week after the booster. Purified CD4$^+$ T cells were cultured with irradiated APCs and 5 μg ml^{-1} of PspA with anti-CD28 and CD49d antibodies for 5 days. The levels of the cytokines, IFN-γ (**a**), IL-4 (**b**), and IL-17A (**c**) in the supernatants were measured. This experiment was repeated in triplicate. Values are shown as the means ± s.d. in each experimental group. $^{**}P < 0.01$ compared between PspA-nanogel and PspA/PBS groups. (**d**) Serum from macaques was collected 1 week after the final primary nasal immunization with PspA-nanogel (#2-#6), PspA alone (#7, #8), or PBS only (#9). Expression levels of PspA-specific serum IgG subclass Abs were determined by using ELISA. APCs, antigen-presenting cells; IFN, interferon; IL, interleukin; PBMC, peripheral blood mononuclear cells.

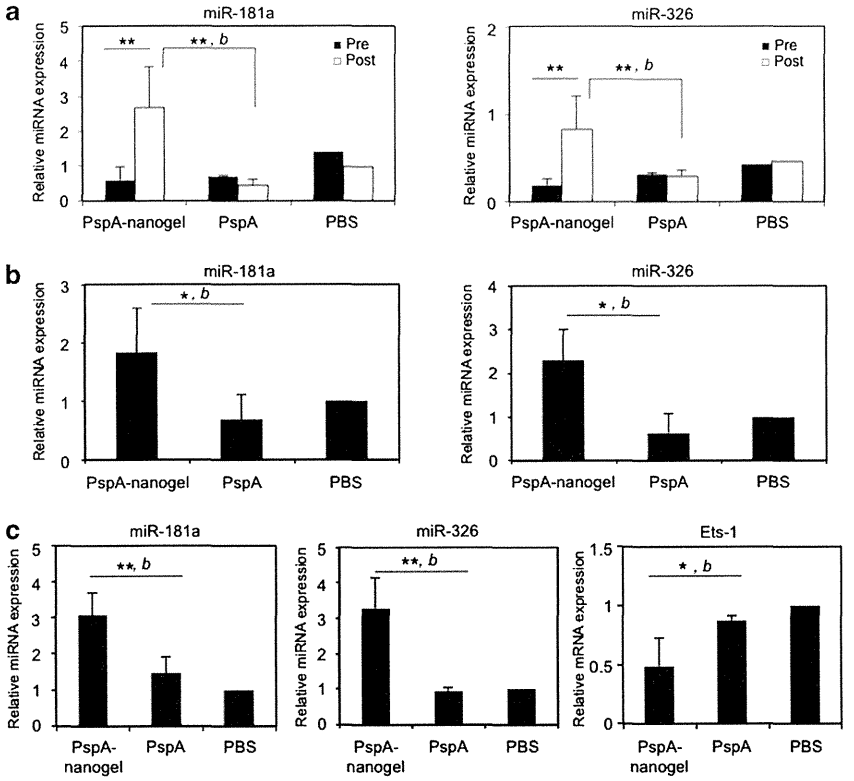

Figure 5 MiRNA expression levels in sera (**a**), nasal tissues (**b**), and lung tissues (**c**) of macaques nasally immunized with PspA-nanogel, PspA alone, or PBS only. Expression levels of the indicated miRNA and Ets-1 mRNA were analyzed by quantitative RT–PCR and normalized to the levels of miR-16 and β-actin, respectively. Values are shown as the means ± s.d. in each experimental group. $^{*}P < 0.05$, $^{**}P < 0.01$ when compared between pre-immunization and post-booster groups. *b*, Compared between PspA-nanogel and PspA/PBS groups in post-booster macaques. MiRNA, microRNA; Pre, pre-immunized serum; Post, post-booster serum.

epithelium layer of macaques. We confirmed the perfect complex formation and the size of PspA-nanogel complex using fluorescence response energy transfer (FRET) analysis and dynamic light scattering (DLS): the cCHP nanogel spontaneously formed nanoparticles after the incorporation of PspA (**Supplementary Figure S1a,b**).[18,19] In addition, consistent with its positive zeta-potential (**Supplementary Figure S1b**), *in vivo* PET and MRI imaging in macaques clearly showed that nasally administered cCHP nanogel carrying [^{18}F]-labeled PspA was more effectively delivered to and continuously retained at the nasal mucosa of macaques when compared with nasally delivered [^{18}F]-PspA alone. These results indicated that the new cationic group-modified cCHP nanogel would be able to efficiently deliver the vaccine antigen to the anionic nasal epithelium following nasal administration in macaques. Indeed, our previous mouse model studies have shown that the nanogel–antigen complex is retained and taken up into the epithelium by endocytosis, where the antigen is released from the nanogel in the epithelium by strong chaperone-like activity. The antigen is then released from the nasal epithelium by exocytosis and subsequently taken up effectively by DCs.[19,21]

Recent studies of nasal vaccines have raised concerns about the deposition and accumulation of candidate vaccine antigens or co-administered mucosal adjuvants in the CNS through direct transport from the nasal cavity to the cerebrum via the olfactory pathways.[29,30] It has also been reported that many peptides and proteins bypass the blood–brain and blood–cerebrospinal fluid barriers to reach the CNS following nasal administration in humans.[31] In this study, we showed that there was no deposition or accumulation of [^{18}F]-PspA in the CNS over a period of up to 6 h after nasal administration of [^{18}F]-PspA-nanogel in macaques. As we validated the detection limit of our PET system for [^{18}F]-protein by direct tissue counting in our previous study,[32] [^{18}F] radioactivity in this study was <0.05 SUV in the cerebrum and olfactory bulbs of the macaques. Therefore, our current results demonstrated that the cCHP delivered nasal PspA vaccine did not reach the CNS of macaques, even though the olfactory epithelium in the nasal cavity is connected to the CNS,[31] thereby confirming the safety of the vaccine in higher mammals.

The mucosal immune system consists of both inductive and effector sites and has a key role in the induction and regulation of dynamic immune responses, including the Th2-type-cell-dependent SIgA response, the mucosal cytotoxic T-cell response, and the Th17-cell-mediated immune regulatory response.[33] In general, IgA in mucosal tissue is thought to have an important role in protection against respiratory pathogens including *S. pneumoniae*.[15–17] In this study, we showed that the PspA-nanogel vaccine also induced mucosal antigen-specific mucosal IgA and systemic IgG Ab responses in the macaques. Especially, serum and BALF IgG, the main isotype of antibody in the lower respiratory compartment, have key roles in survival against lethal challenge with *S. pneumoniae*.[34] Importantly, the macaque IgG antibodies to PspA, which are supported by CD4$^+$ Th2-type cytokine IL-4, possessed protective activity against *S. pneumoniae*. When mice were systemically challenged with *S. pneumoniae* Xen10 or 3JYP2670 after mice passively immunized with macaques' sera containing PspA-specific Abs, they showed complete protection. Our findings indicate that this protection is clearly due to antibody-mediated immunity to PspA. These results are consistent with those of a previous study in mice showing that nasal vaccination induces functional CD4$^+$ Th2-type cytokine-mediated IgG Ab responses, which are sufficient to provide appropriate protection in the absence of Th1-type cytokine responses.[16] In addition, induction of the BALF IgG responses is essential, as antigen-specific IgG is known to exert protection at the alveolar level following to promote phagocytosis and prevents local dissemination of the pneumococcus and its passage into the blood.[34] These results demonstrated that the nasal PspA-nanogel vaccine effectively induced PspA-specific serum IgG with protective activity in addition to SIgA Ab immune responses in nonhuman primates.

Recent studies have shown that specific miRNAs are involved in T-cell and B-cell development, differentiation, and regulatory functions.[24,35] Especially, miR-181a is highly expressed in mature T cells and has an important effect on the positive and negative selection process by controlling the strength of TCR signaling during thymic development of T cells for subsequent Th1 and Th2 differentiation, indicating that miR-181a modulates T-cell development.[36] In this study, the expression levels of miR-181a in the serum and respiratory tract tissues, including nasal tissues and lungs, were significantly higher in macaques nasally immunized with PspA-nanogel than in those given PspA alone or PBS only, indicating that miRNAs are implicated in adaptive immunity by controlling the activation of T cells after nasal immunization with PspA-nanogel in nonhuman primates. Furthermore, we showed that the levels of miR-155, which is required for the production of high-affinity IgG1 Abs, were increased in PspA-nanogel-immunized macaques (**Supplementary Figure S2a–c**).[37] These results indicated that PspA-nanogel-induced Th2 cytokine response was mediated through the increased expression of miR-155.

MiR-181a is also highly expressed in B cells and within bone marrow cells and germinal center B cells, where it promotes the differentiation of hematopoietic stem cells into B cells.[24,38] To explore the roles of other miRNAs that are also highly expressed in germinal center B cells and are essential for adult B-cell development, we examined the expression of the miR-17-92 cluster.[39,40] The miR-17-92 cluster regulates follicular helper T cell (Tfh cell) differentiation by controlling the migration of CD4$^+$ T cells into B-cell follicles,[41] suggesting that these miRNAs have an important role in the production of antigen-specific SIgA Ab. We found here that not only miR-181a expression but also miR-17-92 cluster expression was markedly increased in the nasal tissues of nasally PspA-nanogel-immunized macaques (**Supplementary Figure S3**). Detection of these mucosal IgA-associated miRNAs in the nasal tissues of nasally PspA-nanogel-immunized macaques

indicates that they contribute substantially to the production of mucosal IgA.

It is well known that IL-17-mediated $CD4^+$ T cells are important for the generation of resistance to mucosal colonization by respiratory pathogens including *S. pneumoniae* in humans and mice.[42,43] Trzcinski *et al.*[44] demonstrated that antigen-specific $CD4^+$ T-cell immunity is sufficient to protect against nasopharyngeal colonization by *S. pneumoniae* in mice. Studies in mice indicated that pulmonary Th17 responses are associated with migration of B cells into airways and with the promotion of polymeric Ig receptor (pIgR) expression by airway epithelial cells.[45] In addition, Th17 cells are a crucial subset of Th cells responsible for inducing the switch of germinal center B cells toward T-cell-dependent IgA production.[46] Furthermore, IL-17-secreting memory Th17 cells increased by human pneumococcal carriage have been reported to enhance innate cellular immunity against pneumococcal challenge.[47] Therefore, it is important to determine whether antigen-specific $CD4^+$ Th17 responses are induced by nasal immunization with PspA-nanogel in nonhuman primates. Recent studies have shown that miR-326-mediated Th17 upregulation might provide the host with a potentiating effect to recruit functional immune cells to local effector sites in response to pathogen attack.[48] We found here that nasal immunization with PspA-nanogel in macaques prompted the generation of IL-17-producing cells in the peripheral blood $CD4^+$ T cells. Furthermore, our miRNA analysis showed that expression levels of Th17-associated miR-326 in the serum, nasal tissues, and lungs were significantly increased and that the expression level of Ets-1 mRNA, a negative regulator of Th17 differentiation, was decreased in the lungs of the PspA-nanogel-vaccinated macaques. Therefore, our finding that miR-326-associated IL-17-secreting $CD4^+$ T cells were generated after nasal vaccination with PspA-nanogel suggests that it would be useful for the development of safe and efficacious nasal vaccines against pneumonia and that serum miR-326 could be used as a biomarker to evaluate vaccine efficacy.

In summary, we demonstrated for the first time that a nasal PspA-nanogel vaccine induced both humoral and cellular immune responses in macaques. These results were supported by increased expression levels of miR-181a and miR-326, which are candidate miRNA biomarkers for induction of mucosal immunity. In addition, a [^{18}F]-PspA PET study showed long-term retention of PspA in the nasal cavity and no deposition of PspA in the CNS of the macaques. Taken together, these findings demonstrate the efficacy and safety of nasal PspA-nanogel vaccine in nonhuman primates. We conclude that the nasal PspA-nanogel vaccine should now be studied in humans for its possible use as an adjuvant-free nasal vaccine.

METHODS

Animals. Eight female naive cynomolgus macaques (*Macaca fascicularis*, 5 years old, ~3 kg) were used for the immunization study and were maintained at the Tsukuba Primate Research Center for Medical Science at the National Institute of Biomedical Innovation (NIBIO, Ibaraki, Japan). In a separate experiment, one naive male rhesus macaque (*M. mulatta*, 5–6 years old, ~5 kg) was used for the PET imaging study, which was conducted at PET Center of Hamamatsu Photonics K.K. To assay antibody protection against *S. pneumoniae*, female CBA/N mice (6 weeks old) were purchased from Japan SLC (Shizuoka, Japan). All experiments were performed in accordance with the Guidelines for Use and Care of Experimental Animals, and the protocol was approved by the Animal Committee of NIBIO, Hamamatsu Photonics K.K., and The University of Tokyo.

Recombinant PspA. Recombinant PspA of *S. pneumoniae* Rx1, which belongs to PspA family 1 and clade 2, was prepared as described previously, with slight modification.[10] In brief, the plasmid encoding PspA/Rx1 (GenBank accession no. M74122; amino acids 1 through 302, pUAB055) was used to transform *E. coli* BL21 (DE3) cells. To construct pUAB055, a 909-bp fragment of PspA from a pneumococcal strain Rx1 was cloned into the pET20b vector (Novagen, Darmstadt, Germany) between the *Nco*I and *Xho*I sites. Recombinant PspA/Rx1 contains the first 302 amino acids of mature PspA plus six poly-histidines added through protein fusion at the C-terminal end. The sonicated cell supernatant was loaded onto a DEAE-Sepharose column (BD Healthcare, Piscataway, NJ) and a nickel affinity column (Qiagen, Valencia, CA), followed by gel filtration on a Sephadex G-100 column (BD Healthcare).

Preparation of recombinant PspA–nanogel complex. The cCHP nanogel (~40 nm size) generated from cationic type of cholesteryl group-bearing pullulan was used for all experiments. This cCHP nanogel contained 20 amino groups per 100 glucose units. The PspA-cCHP nanogel complex for each immunization was prepared by mixing 25 μg of PspA with cCHP at a 1:5 molecular ratio (59.45 μl per macaque) and incubating for 1 h at 46 °C. FRET was determined with an FP-6500 fluorescence spectrometer (JASCO, Tokyo, Japan) with FITC-conjugated PspA and TRITC-conjugated cCHP nanogel.[18,19] The hydrodynamic radius was assessed by means of DLS and the zeta-potential of cCHP carrying or not carrying, PspA was determined with a Zetasizer Nano ZS instrument (Malvern Instruments, Worcestershire, UK).[18,19]

Nasal immunization and sample collection. Cynomolgus macaques were nasally immunized five times at 2-week intervals with PspA-nanogel under ketamine anesthesia. For the control group, macaques were nasally administered with 25 μg of PspA alone, or PBS only. Eight months after the final immunization, the macaques were nasally boosted with the same amount of PspA-nanogel, PspA alone or PBS only. Serum, nasal wash, and BALF were collected before primary immunization, 1 week after each immunization, 2, 4, 6, and 8 months after the final immunization, and 2 weeks after receipt of the booster.

PspA-specific ELISA. The antigen-specific Ab responses were analyzed by ELISA as described previously.[21] In brief, 96-well plates were coated with 1 μg ml^{-1} PspA in PBS overnight at 4 °C. After blocking with 1 % BSA in PBS-Tween, twofold serial dilutions of samples were added and incubated for 2 h at room temperature (RT). After washing of the samples, horseradish peroxidise (HRP)-conjugated goat anti-monkey IgG (Nordic Immunological Laboratory, Tilburg, The Netherlands) or HRP-conjugated goat anti-monkey IgA (Cortex Biochem, San Leandro, CA) diluted 1:1,000 was added and incubated for 2 h at room temperature. For subclass analysis, sheep anti-human IgG1 and IgG2 (Binding Site, Birmingham, UK) and HRP-conjugated donkey anti-sheep IgG (Rockland, Limerick, PA) were used for detection. The reaction was developed with the use of TMB Microwell Peroxidase Substrate System (XPL, Gaithersburg, MD). End-point titers were expressed as the reciprocal $\log_2$ of the last dilution that gave an OD_{450} of 0.1 greater than the negative control.

Passive protection of mice with macaques' serum samples. Pooled serum samples from macaques nasally immunized with PspA-

nanogel, PspA alone, or PBS only were diluted with PBS (1:20) and injected into CBA/N mice via the intraperitoneal route (100 µl per mouse). Four hours later, all groups of mice were challenged with 1.5×10^4 CFU *S. pneumoniae* Xen 10 ($LD_{50} = 2 \times 10^2$ CFU for CBA/N mice) or 1×10^3 CFU *S. pneumoniae* 3JYP2670 strain ($LD_{50} = 7 \times 10^2$ CFU for CBA/N mice) via the intravenous route and observed daily for death for 2 weeks. Information about *S. pneumoniae* strains is available in **Supplementary Materials**.

PspA-specific CD4$^+$ T-cell responses. One week after the macaques had received the booster, lymphocytes were isolated from the peripheral blood by using Ficoll-Paque PLUS (GE Healthcare, Little Chalfont, UK). We could not separate the lymphocytes from two macaques (#3 and #6). After washing of the samples, CD4$^+$ T cells were purified by using CD4 microbeads and magnetic cell sorting (AutoMACS; Miltenyi Biotec, Auburn, CA). The cells remaining after the removal of CD4$^+$ and CD8$^+$ T cells (by using CD8 microbeads) were used as antigen-presenting cells after irradiation at 3,000 rad. Purified CD4$^+$ T cells (1×10^5 cells/well) and antigen-presenting cells (0.5×10^5 cells/well) were resuspended in RPMI 1640 (Nacalai Tesque, Kyoto, Japan) supplemented with 10 % FCS and penicillin-streptomycin (Gibco, Carlsbad, CA), and were cultured in 24-well plates for 5 days in the presence of 5 µg ml^{-1} PspA with anti-CD28 (clone CD28.2) and CD49d (clone 9F10) antibodies (0.5 µg ml^{-1} each; eBioscience, San Diego, CA) at 37 °C in 5% CO_2. Supernatants were then collected. The concentrations of the cytokines, IFN-γ, IL-4, and IL-17 in the supernatants were measured with a Monkey Singleplex Bead Kit (Invitrogen, Carlsbad, CA) and Bio-Plex 200 (Bio-Rad, Hercules, CA).

Synthesis of [^{18}F]-PspA. Purified PspA was radiolabeled by conjugation with *N*-succinimidyl-4-[^{18}F]fluorobenzoate ([^{18}F]SFB), which reacts with free amino groups, including the N-terminal and ε-Lys amino groups in the protein, as described previously.[19,32] The product was purified by gel-permeation chromatography (Superose 12, PBS, 1 ml min^{-1}), and the radioactive peak that eluted at 12.7 min was collected. The 615 MBq [^{18}F]-PspA was obtained at 150 min from the end of bombardment. The radiochemical purity and the decay-corrected radiochemical yield were 100 and 2.95%, respectively. The specific activity was 1,798 to 4,045 MBq mg^{-1} protein.

PET/MRI imaging in rhesus macaques. Because the half-life of [^{18}F] is only 110 min, we used the same naive macaque for nasal [^{18}F]-PspA-nanogel or [^{18}F]-PspA-PBS administration with a 1-week interval between administrations. After nasal administration of 50 MBq per 700 µl of [^{18}F]-PspA-nanogel or [^{18}F]-PspA-PBS (350 µl in each nostril), the macaque's head was tilted back for 10 min and then scanned in an upright position. PET scans were conducted for 345 min with frames of 25 × 3 min, followed by 27 × 10 min, with the use of a high-resolution animal PET scanner (SHR-7700; Hamamatsu Photonics, Shizuoka, Japan). MRI images were recorded with Signa Excite HDxt (3T; GE Healthcare) to identify the cerebrum regions.

Image data analysis. PET data were analyzed by means of the PMOD software package (PMOD Technologies, Zurich, Switzerland). Each PET image was superimposed on the corresponding MRI data to identify the volume of interest. Time-activity curves (TACs) of PET/MRI images were expressed as % remaining dose.

MiRNA expression levels in serum and respiratory tract tissues. Serum samples were collected before primary immunization and after booster with PspA-nanogel, PspA alone, or PBS only. The respiratory tract tissues, which included nasal epithelial and lung samples, were collected after booster immunization with PspA-nanogel, PspA alone, or PBS only. Total RNAs were isolated from serum by using TRIzol LS reagent, and from nasal tissue or lung by using TRIzol reagent (Invitrogen) following the manufacturer's protocol. All the miRNAs in the sample were polyadenylated by using poly(A) polymerase and ATP (Invitrogen). Following polyadenylation, SuperScript III RT and a specially designed Universal RT Primer (Invitrogen) were used to synthesize cDNA from the tailed miRNA population. Each of the first-strand cDNAs was analyzed by quantitative RT-PCR with Fast SYBR Green Master Mix and Step One Plus Real-Time PCR System (Applied Biosystems, Carlsbad, CA). The expression levels were normalized to miR-16, which is a commonly used internal control for miRNA expression.[49,50]

Analysis of Ets-1 expression. After total RNAs were isolated from lung tissue, cDNA was synthesized by using PrimeScript RT Master Mix (Takara, Shiga, Japan) following the manufacturer's protocol. The cDNA was analyzed by quantitative RT–PCR with Fast SYBR Green Master Mix and Step One Plus Real-Time PCR System (Applied Biosystems). The PCR primers were used as follows: Ets-1: F, 5′-TGG AGTCAACCCAGCCTATC-3′ and R, 5′-TCTGCAAGGTGTCTGTC TGG-3′; β-actin: F, 5′-TGACGTGGACATCCGCAAAG-3′ and R, 5′-CTGGAAGGTGGACAGCGAGG-3′. The expression levels were normalized to that of β-actin.

Statistical analysis. The results are presented as means ± s.d. Student's *t*-test was used for comparisons among groups. The *P* values <0.05 or <0.01 were considered to indicate statistical significance.

SUPPLEMENTARY MATERIAL is linked to the online version of the paper at http://www.nature.com/mi

ACKNOWLEDGMENTS

This work was supported by the Ministry of Health, Labour, and Welfare of Japan (Y. Y.), Global Center of Excellence Program "Center of Education and Research for the Advanced Genome—Based Medicine—For personalized medicine, the control of worldwide infectious diseases—"MEXT" Japan (Y.F. and H.K.), the Ministry of Education, Culture, Sports, Science, and Technology of Japan (Grant-in-Aid for Scientific Research S [23229004], H.K.), and the Core Research for Evolutional Science and Technology Program of the Japan Science and Technology Agency (H.K.). We are grateful to Drs. Natsumi Takeyama, Koji Kashima, and Tatsuhiko Azegami and Mr. Yuji Suzuki for their useful discussions and technical support.

DISCLOSURE

The authors declare no conflict of interest.

REFERENCES

1. Jackson, L.A. & Janoff, E.N. Pneumococcal vaccination of elderly adults: new paradigms for protection. *Clin. Infect. Dis.* **47**, 1328–1338 (2008).
2. Nuorti, J.P. & Whitney, C.G. Prevention of pneumococcal disease among infants and children - use of 13-valent pneumococcal conjugate vaccine and 23-valent pneumococcal polysaccharide vaccine - recommendations of the Advisory Committee on Immunization Practices (ACIP). *MMWR Recomm. Rep.* **59**, 1–18 (2010).
3. Oosterhuis-Kafeja, F., Beutels, P. & Van Damme, P. Immunogenicity, efficacy, safety and effectiveness of pneumococcal conjugate vaccines (1998-2006). *Vaccine* **25**, 2194–2212 (2007).
4. Dagan, R. *et al.* Reduction of nasopharyngeal carriage of Streptococcus pneumoniae after administration of a 9-valent pneumococcal conjugate vaccine to toddlers attending day care centers. *J. Infect. Dis.* **185**, 927–936 (2002).
5. Dagan, R. *et al.* Comparative immunogenicity and efficacy of 13-valent and 7-valent pneumococcal conjugate vaccines in reducing nasopharyngeal colonization: a randomized double-blind trial. *Clin. Infect. Dis.* **57**, 952–962 (2013).
6. Croney, C.M., Coats, M.T., Nahm, M.H., Briles, D.E. & Crain, M.J. PspA family distribution, unlike capsular serotype, remains unaltered following introduction of the heptavalent pneumococcal conjugate vaccine. *Clin. Vaccine Immunol.* **19**, 891–896 (2012).
7. Pilishvili, T. *et al.* Sustained reductions in invasive pneumococcal disease in the era of conjugate vaccine. *J. Infect. Dis.* **201**, 32–41 (2010).

8. Berry, A.M., Yother, J., Briles, D.E., Hansman, D. & Paton, J.C. Reduced virulence of a defined pneumolysin-negative mutant of *Streptococcus pneumoniae*. *Infect. Immun.* **57**, 2037–2042 (1989).
9. McDaniel, L.S. *et al.* Use of insertional inactivation to facilitate studies of biological properties of pneumococcal surface protein A (PspA). *J. Exp. Med.* **165**, 381–394 (1987).
10. Briles, D.E. *et al.* Intranasal immunization of mice with a mixture of the pneumococcal proteins PsaA and PspA is highly protective against nasopharyngeal carriage of *Streptococcus pneumoniae*. *Infect. Immun.* **68**, 796–800 (2000).
11. Nguyen, C.T., Kim, S.Y., Kim, M.S., Lee, S.E. & Rhee, J.H. Intranasal immunization with recombinant PspA fused with a flagellin enhances cross-protective immunity against *Streptococcus pneumoniae* infection in mice. *Vaccine* **29**, 5731–5739 (2011).
12. McCool, T.L., Cate, T.R., Moy, G. & Weiser, J.N. The immune response to pneumococcal proteins during experimental human carriage. *J. Exp. Med.* **195**, 359–365 (2002).
13. Kono, M., Hotomi, M., Hollingshead, S.K., Briles, D.E. & Yamanaka, N. Maternal immunization with pneumococcal surface protein A protects against pneumococcal infections among derived offspring. *PLoS One* **6**, e27102 (2011).
14. Fukuyama, Y. *et al.* A combination of Flt3 ligand cDNA and CpG oligodeoxynucleotide as nasal adjuvant elicits protective secretory-IgA immunity to *Streptococcus pneumoniae* in aged mice. *J. Immunol.* **186**, 2454–2461 (2011).
15. Ferreira, D.M. *et al.* Characterization of protective mucosal and systemic immune responses elicited by pneumococcal surface protein PspA and PspC nasal vaccines against a respiratory pneumococcal challenge in mice. *Clin. Vaccine Immunol.* **16**, 636–645 (2009).
16. Fukuyama, Y. *et al.* Secretory-IgA antibodies play an important role in the immunity to *Streptococcus pneumoniae*. *J. Immunol.* **185**, 1755–1762 (2010).
17. Janoff, E.N. *et al.* Killing of *Streptococcus pneumoniae* by capsular polysaccharide-specific polymeric IgA, complement, and phagocytes. *J. Clin. Invest.* **104**, 1139–1147 (1999).
18. Ayame, H., Morimoto, N. & Akiyoshi, K. Self-assembled cationic nanogels for intracellular protein delivery. *Bioconjug. Chem.* **19**, 882–890 (2008).
19. Nochi, T. *et al.* Nanogel antigenic protein-delivery system for adjuvant-free intranasal vaccines. *Nat. Mater.* **9**, 572–578 (2010).
20. Yuki, Y. *et al.* Nanogel-based antigen-delivery system for nasal vaccines. *Biotechnol. Genet. Eng. Rev.* **29**, 61–72 (2013).
21. Kong, I.G. *et al.* Nanogel-based PspA intranasal vaccine prevents invasive disease and nasal colonization by *Streptococcus pneumoniae*. *Infect. Immun.* **81**, 1625–1634 (2013).
22. Baltimore, D., Boldin, M.P., O'Connell, R.M., Rao, D.S. & Taganov, K.D. MicroRNAs: new regulators of immune cell development and function. *Nat. Immunol.* **9**, 839–845 (2008).
23. O'Connell, R.M., Rao, D.S., Chaudhuri, A.A. & Baltimore, D. Physiological and pathological roles for microRNAs in the immune system. *Nat. Rev. Immunol.* **10**, 111–122 (2010).
24. Zhu, S., Pan, W. & Qian, Y. MicroRNA in immunity and autoimmunity. *J. Mol. Med.* **91**, 1039–1050 (2013).
25. Cobb, B.S. *et al.* T cell lineage choice and differentiation in the absence of the RNase III enzyme Dicer. *J. Exp. Med.* **201**, 1367–1373 (2005).
26. Muljo, S.A. *et al.* Aberrant T cell differentiation in the absence of Dicer. *J. Exp. Med.* **202**, 261–269 (2005).
27. Koralov, S.B. *et al.* Dicer ablation affects antibody diversity and cell survival in the B lymphocyte lineage. *Cell* **132**, 860–874 (2008).
28. Kitano, S. *et al.* HER2-specific T-cell immune responses in patients vaccinated with truncated HER2 protein complexed with nanogels of cholesteryl pullulan. *Clin. Cancer Res.* **12**, 7397–7405 (2006).
29. van Ginkel, F.W., Jackson, R.J., Yuki, Y. & McGhee, J.R. Cutting edge: the mucosal adjuvant cholera toxin redirects vaccine proteins into olfactory tissues. *J. Immunol.* **165**, 4778–4782 (2000).
30. Yuki, Y. & Kiyono, H. Mucosal vaccines: novel advances in technology and delivery. *Expert Rev. Vaccines* **8**, 1083–1097 (2009).
31. Illum, L. Is nose-to-brain transport of drugs in man a reality? *J. Pharm. Pharmacol.* **56**, 3–17 (2004).
32. Yuki, Y. *et al.* In vivo molecular imaging analysis of a nasal vaccine that induces protective immunity against botulism in nonhuman primates. *J. Immunol.* **185**, 5436–5443 (2010).
33. Fukuyama, Y. *et al.* Novel vaccine development strategies for inducing mucosal immunity. *Expert Rev. Vaccines* **11**, 367–379 (2012).
34. Twigg, H.L. 3rd Humoral immune defense (antibodies): recent advances. *Proc. Am. Thorac. Soc.* **2**, 417–421 (2005).
35. Baumjohann, D. & Ansel, K.M. MicroRNA-mediated regulation of T helper cell differentiation and plasticity. *Nat. Rev. Immunol.* **13**, 666–678 (2013).
36. Li, Q.J. *et al.* miR-181a is an intrinsic modulator of T cell sensitivity and selection. *Cell* **129**, 147–161 (2007).
37. Vigorito, E. *et al.* microRNA-155 regulates the generation of immunoglobulin class-switched plasma cells. *Immunity* **27**, 847–859 (2007).
38. Chen, C.Z., Li, L., Lodish, H.F. & Bartel, D.P. MicroRNAs modulate hematopoietic lineage differentiation. *Science* **303**, 83–86 (2004).
39. Tan, L.P. *et al.* miRNA profiling of B-cell subsets: specific miRNA profile for germinal center B cells with variation between centroblasts and centrocytes. *Lab. Invest.* **89**, 708–716 (2009).
40. Ventura, A. *et al.* Targeted deletion reveals essential and overlapping functions of the miR-17 through 92 family of miRNA clusters. *Cell* **132**, 875–886 (2008).
41. Kang, S.G. *et al.* MicroRNAs of the miR-17-92 family are critical regulators of T(FH) differentiation. *Nat. Immunol.* **14**, 849–857 (2013).
42. Lu, Y.J. *et al.* Interleukin-17A mediates acquired immunity to pneumococcal colonization. *PLoS Pathog.* **4**, e1000159 (2008).
43. Malley, R. *et al.* $CD4^+$ T cells mediate antibody-independent acquired immunity to pneumococcal colonization. *Proc. Natl. Acad. Sci. USA* **102**, 4848–4853 (2005).
44. Trzcinski, K. *et al.* Protection against nasopharyngeal colonization by *Streptococcus pneumoniae* is mediated by antigen-specific $CD4^+$ T cells. *Infect. Immun.* **76**, 2678–2684 (2008).
45. Jaffar, Z., Ferrini, M.E., Herritt, L.A. & Roberts, K. Cutting edge: lung mucosal Th17-mediated responses induce polymeric Ig receptor expression by the airway epithelium and elevate secretory IgA levels. *J. Immunol.* **182**, 4507–4511 (2009).
46. Hirota, K. *et al.* Plasticity of Th17 cells in Peyer's patches is responsible for the induction of T cell-dependent IgA responses. *Nat. Immunol.* **14**, 372–379 (2013).
47. Wright, A.K. *et al.* Experimental human pneumococcal carriage augments IL-17A-dependent T-cell defence of the lung. *PLoS Pathog.* **9**, e1003274 (2013).
48. Du, C. *et al.* MicroRNA miR-326 regulates TH-17 differentiation and is associated with the pathogenesis of multiple sclerosis. *Nat. Immunol.* **10**, 1252–1259 (2009).
49. Chang, K.H., Mestdagh, P., Vandesompele, J., Kerin, M.J. & Miller, N. MicroRNA expression profiling to identify and validate reference genes for relative quantification in colorectal cancer. *BMC Cancer* **10**, 173 (2010).
50. Mizuno, H. *et al.* Identification of muscle-specific microRNAs in serum of muscular dystrophy animal models: promising novel blood-based markers for muscular dystrophy. *PLoS One* **6**, e18388 (2011).

Comparative Medicine
Copyright 2015
by the American Association for Laboratory Animal Science

Vol 65, No 1
February 2015
Pages 1–7

Original Research

Detection and Quantification of Male-Specific Fetal DNA in the Serum of Pregnant Cynomolgus Monkeys (*Macaca fascicularis*)

Lubna Yasmin,[1] Jun-ichiro Takano,[1] Yasushi Nagai,[2] Junko Otsuki, [1,2,3] and Tadashi Sankai[1,*]

Because of their developmental similarities to humans, nonhuman primates are often used as a model to study fetal development for potential clinical applications in humans. The detection of fetal DNA in maternal plasma or serum offers a source of fetal genetic material for prenatal diagnosis. However, no such data have been reported for cynomolgus monkeys (*Macaca fascicularis*), an important model in biomedical research. We have developed a specific, highly sensitive PCR system for detecting and quantifying male-specific fetal DNA in pregnant cynomolgus monkeys. We used multiplex quantitative real-time PCR to analyze cell-free DNA in maternal blood serum obtained from 46 pregnant monkeys at gestational weeks 5, 12, and 22. The presence of *SRY* gene and DYS14 Y chromosomal sequences was determined in 28 monkeys with male-bearing pregnancies. According to confirmation of fetal sex at birth, the probe and primers for detecting the Y chromosomal regions at each time point revealed 100% specificity of the PCR test and no false-positive or false-negative results. Increased levels of the *SRY*-specific sequences (mean, 4706 copies/mL serum DNA; range, 1731 to 12,625) and DYS14-specific sequences (mean, 54,814 copies/mL serum DNA; range, 4175–131,250 copies) were detected at week 22. The *SRY*- and DYS14-specific probes appear to be an effective combination of markers in a multiplex PCR system. To our knowledge, this report is the first to describe the detection of cell-free DNA in cynomolgus monkeys.

Abbreviation: C_t, threshold cycle.

Analysis of cell-free circulating nucleic acids in human maternal plasma or serum has led to the development of risk-free methods for prenatal genetic diagnosis and the assessment of several fetal and maternal conditions, for example, sex determination for paternally inherited diseases, pregnancy-associated complications, sex-linked disorders for ambiguous genitalia, and embryo tracking.[1,4,12,14,18,19] Technical challenges associated with detecting fetal DNA arise due to the low concentration of fetal DNA in maternal plasma during pregnancy and the difficulty of differentiating the genetic material of the fetus from that of the mother.[5,13,20] Fetal sex determination using sequences derived from the Y chromosome only is relatively simple and has a reported accuracy rate in humans of approximately 99.0% at 7 wk of gestation and 100% after 20 wk, depending on the protocol and methods used.[3,5,17,20] In other species, researchers have used real-time PCR assays during pregnancy to predict fetal sex from cell-free DNA at an accuracy of 100%.[9,10,11] Cell-free fetal DNA in the maternal circulation represents only 3% to 6% of the total free DNA obtained from plasma throughout pregnancy; however, this percentage is variable between pregnancies.[5,13,20]

Received: 09 Jul 2014. Revision requested: 10 Aug 2014. Accepted: 18 Sep 2014.
[1]Tsukuba Primate Research Center, National Institute of Biomedical Innovation, Tsukuba, Ibaraki, Japan, [2]Department of Obstetrics and Gynecology, Nagai Clinic, Saitama, Japan, and [3]Hanabusa Women's Clinic, Kobe, Hyogo, Japan
**Corresponding author. Email: t-sankai@nibio.go.jp*

In clinical biomedical research, it is essential to develop animal models for human diseases to reveal their mechanisms.[16,22] Continued progress in surgical intervention and molecular medicine suggests that it may soon be possible to develop potential treatments or even cures for several fetal genetic diseases at an early stage of pregnancy.[15] Fetal developmental research during early pregnancy might be facilitated by using cell-free fetal DNA in the maternal blood rather than other methods, such as serum screening and ultrasonography. Nonhuman primates, especially macaques, are useful model animals for studying fetal development because of the similarity of the reproductive characteristics, placental structure, and developmental events between these animals and humans.[9,10] These developmental similarities highlight the importance of the study of cell-free fetal DNA in nonhuman primates and its usefulness as a marker to obtain genetic information about the fetus.

In the current study, we investigated the presence of cell-free fetal DNA in the maternal plasma of cynomolgus monkeys by developing and using a standardized PCR system. To this end, we selected the *SRY* (sex-determining region Y) gene and DYS14 sequences of the cynomolgus monkey to use as sex-associated markers. The Y chromosome-specific sequences in the single-copy sex determination region of *SRY* and the multicopy (thus yielding increased sensitivity) sequences of DYS14 in the *TSPY* (testis-specific protein, Y-linked) gene have had wide clinical use in humans as molecular markers for detecting and quantifying

cell-free fetal DNA.[3,7] In addition, *TSPY* has been used in bovines for detecting cell-free fetal DNA[2] and in rhesus macaques for long-term evaluation of microchimerism.[8] Given the reports of fetal sex determination in rhesus macaques[9,10] and sheep[11] by analyzing Y chromosome-specific sequences from cell-free DNA, we hypothesized that we could predict the fetal sex of cynomolgus monkeys at different stages of gestation. This information has been extremely useful in optimizing the design of experimental studies in biomedical research and in managing a nonhuman primate breeding colony.[10] Because cynomolgus and rhesus macaques are closely related members of the same genus, the current experiments are similar to a previous study.[9]

We developed an efficient 2-color multiplex PCR system to detect and quantify fetal DNA in the maternal serum of cynomolgus monkeys during pregnancy. We used 2 loci on the Y chromosome in a single PCR test to minimize the likelihood of false-positive signals. Here we report the results of detection and analysis of fetal DNA at various weeks of gestation and evaluate our PCR system for its ability to determine fetal sex from pregnant monkeys' cell-free DNA.

Materials and Methods

Blood sampling and serum separation. The IACUC of the National Institute of Biomedical Innovation approved the protocol. This research adhered to the legal requirements of Primate Society of Japan's principles for the ethical treatment of primates. The study animals (*Macaca fascicularis*) were bred and maintained at Tsukuba Primate Research Center. Monkey-rearing rooms were rectangular, and individual cages were installed on the long sides of the room. Animals were housed individually on a 12:12-h light:dark cycle. Ambient temperature in the rooms was kept at approximately 25 °C, and humidity was set at 50% to 60%. Monkeys were provided with apples in the morning, commercial chow twice daily, and water ad libitum. We followed 3 groups of monkeys: the first group (n = 11) was tested at 5 wk of gestation, the second group (n = 15) at 12 wk, and the third group (n = 15) at 22 wk. We also followed a group of 5 monkeys that were monitored continuously and tested at all 3 stages of gestation. The sex of the fetus resulting from each of the pregnancies was recorded at birth. For blood sampling, each dam was anesthetized by using ketamine hydrochloride (dose, 10 to 15 mg/kg; Ketalar, Sankyo, Tokyo, Japan). Blood (2 to 5 mL) was collected by syringe from pregnant monkeys during weeks 5, 12, and 22 of gestation. For positive and negative controls, we collected blood from male and female monkeys to extract genomic DNA. Serum samples, obtained by centrifuging the blood at 1700 × *g* for 15 min, were either used immediately for DNA extraction or stored at –80 °C until needed.

DNA extraction and detecting the specificity of primers. DNA was extracted from 400 µL of serum using the MagNA Pure Compact Nucleic Acid Isolation Kit I (Roche, Mannheim, Germany). To avoid contamination, we used fully automated nucleic acid extraction system according to the manufacturer's instructions. Total blood DNA was extracted from male and female samples for the positive and negative control by using a QIAamp DNA Blood Mini/Midi Kit (Qiagen, Hilden, Germany) according to the manufacturer's instructions. DNA from serum was eluted into a final volume of 50 µL and used as a PCR template.

We designed primers and probes for a 2-color multiplex *Taq*Man PCR assay according to the parameters defined by Beacon Designer 7.9 (Premiere Biosoft International, Palo Alto, CA) was synthesized and purified by Greiner Bio-One (Tokyo, Japan), using *SRY* and DYS14 sequence data from rhesus monkeys (GenBank accession nos. AC217136 and AC240711; Table 1). To evaluate this assay, we constructed standard plasmids containing the *SRY* gene and DSY14 sequences; we used these plasmids as templates to assess the primer sets, which were designed to bind to the flanking regions of the sequences (Table 1). These primers amplified the expected 122- and 95-bp target products specific to *SRY* and DYS14, respectively. A homology search of human and macaque sequences in GenBank using the DYS14 primers and probe sequences that we designed revealed 85% sequence homology with the human *TSPY* gene (accession no., pJA923) and 100% homology with the sequences of the entire Y chromosome and *TSPY* gene (accession nos., AC240711 and AB001421, respectively) in *M. mulatta* and *M. fuscata*. Conventional PCR analysis using genomic male and female DNA as templates was carried out to determine the specificity of designed primers. The total reaction volume was 25 µL. PCR with ExTaq DNA polymerase (Takara Bio, Otsu, Japan) with initial denaturation at 94 °C for 3 min, followed by 35 cycles of 94 °C for 30 s, 60 to 63 °C for 30 s, and 72 °C for 30 s for extension. A final elongation step at 72 °C for 5 min was performed before maintaining the reaction at 4 °C. The amplicons were verified by 1% agarose gel electrophoresis.

Construction of a standard curve and selection of PCR conditions. To determine the detection limits of the PCR assay from a standard curve, we obtained the recombinant *SRY* gene and Y chromosome-specific sequence DYS14 by using male genomic DNA as PCR template. Amplification of 1 kb of the *SRY* gene and DYS14 was performed by using conventional PCR. Purification of the amplified product was carried out by using the NucleoSpin Gel and PCR Clean-Up gel extraction kit (Takara Bio) according to the manufacturer's instructions. The purified product was ligated into the pGEMT vector (Promega, Madison, WI) at 16 °C overnight. The ligation mixture was added to *ECOS Escherichia coli* JM109 competent cells (NIPPON GENE, Toyama, Japan). After PCR analysis, positive clones were designated as the recombinant plasmids pGEMT/SRY and pGEMT/DYS14. Sequences were confirmed by using the 3130xl Genetic Analyzer (Applied Biosystems). Plasmid DNA was extracted from bacteria by using a plasmid midi kit (Qiagen, Valencia, CA). DNA from the plasmids was prepared at a concentration of 10^{10} copies/µL in 1× Tris–EDTA buffer (pH 8.0) followed by serial 10-fold dilutions from 10^5 to 10^0 copies per reaction, which were used to generate a standard curve that enabled copy number to be determined from the threshold cycle (C_t) value obtained. This curve permitted absolute quantification of the number of *SRY* and DYS14 copies in fetal cell-free DNA from the maternal blood sample through comparison with the number of copies of plasmid DNA detected in the same reaction by using C_t values. Primer pairs and reaction conditions were optimized by using control male genomic DNA and pGEMT/SRY and pGEMT/DYS14 plasmids as a template pool before amplification of the samples.

Detection of cell-free DNA by real-time PCR. For real-time PCR analysis of cell-free fetal DNA, reaction tubes at 5 wk of pregnancy contained 100 µL, including 40 µL DNA template, 1 µL of each 20 µM primer, 0.5 µL of each 20 µM probe for *SRY* and DYS14, 50 µL of IQ Super mix (Bio-Rad Laboratories, Hercules, CA), and 5 µL of Tris–EDTA buffer or distilled water. For assays done at 12 wk (reaction volume, 50 µL), each tube contained 20

Table 1. *SRY* gene and DYS14-specific primers and probes used in the real-time PCR assay and plasmid construction. The Y chromosome-specific sequence DYS14 was extracted from AC240711 *M. mulatta* BAC clone CH250-434B12 (GenBank). *SRY* gene primers and probe were extracted from AC217136 *M. mulatta* BAC clone CH250-228N17 (GenBank)

Name	Direction	Sequence (5′ to 3′)
FMSRY	Sense	TCC AGG AGG CAC AGA AAC TA
RMSRY	Antisense	AGA GGG ATC TGC CGG AAG
FMDYS14	Sense	GGA TGG AGT CTC TAC AGG AGG
RMDYS14	Antisense	CGC CAT TAT GTC ATC CGC TC
SRY	Probe	FAM–AGC ATC TTC GCC TTC CGA CGA GGT–BHQ1
DYS14	Probe	HEX–CCC AAA GCT ACC TGC TCG CTC TGC–BHQ1
FpSRY	Sense	TGG TTG GGC GGA GTT GAG AG
RpSRY	Antisense	GGCGGGATCACTTCTGGATG
FpDYS14	Sense	GCTCCTGGTGCCCTTTGGTC
RpDYS14	Antisense	TGTGAGGCTGACCGCACTGA

μL DNA template, 0.5 μL of each 20 μM primer, 0.25 μL of each 20 μM probe for *SRY* and DYS14, 25 μL IQ Super mix (Bio-Rad Laboratories), and 3.5 μL Tris–EDTA buffer or distilled water. At 22 wk of pregnancy, assay tubes each contained 25 μL total, comprising 2 μL DNA template, 0.25 μL of each 20 μM primer, 0.125 μL of each 20 μM probe for *SRY* and DYS14, 12.5 μL of IQ Super mix (Bio-Rad Laboratories), and 9.75 μL of Tris–EDTA buffer or distilled water.

Amplification parameters were: initial denaturation for enzyme activation at 95 °C for 3 min, followed by 55 cycles of denaturation at 95 °C for 10 s and annealing and extension at 63 °C for 30 s in an iQ5 real-time PCR detection system (Bio-Rad). Multiplex quantitative PCR was optimized with DNA from constructed plasmids, and genomic DNA from individual male and female monkeys was used for controls. Results are presented as the amount of DNA in genome-equivalent copies per mL of serum. The C_t values reflect the linear phase in the amplification curve used for quantification of the template input. All PCR tests were performed duplicate or triplicate. Samples were considered positive for *SRY* and DYS14 when results were confirmed by in least 2 tubes in duplicate or triplicate tests.

Statistical analysis. All parameters were calculated by using real-time PCR data from fetal DNA and the iQ5 optical system software (version 1.0.1384.0CR, BioRad). Results are expressed as means based on the mean C_t values. The coefficient of regression (r^2) was calculated from linearity data of the standard curve. The efficiency of each PCR primer–probe set was calculated from the standard curve by using the autoefficiency function of the iQ5 software. The Student *t* test was used to assess differences in *SRY* and DYS14 average copy number between weeks 5 and 12 and between weeks 12 and 22 of gestation. *P* values less than 0.05 were considered significant.

Results

Specificity and lower limit of detection of the PCR assay for the detection of *SRY* and DYS14. We performed conventional PCR analysis of genomic DNA from both male and female cynomolgus monkeys as a control and were successful in detecting male-specific bands. The specific primers yielded the expected 122-bp and 95-bp bands for *SRY* and DYS14, respectively, after gel electrophoresis (data not shown). Real-time PCR analysis using the selected primers and probes and control male and female genomic DNA led to effective amplification of male-specific *SRY* and DYS14 sequences only from male DNA. No amplification products were generated from genomic DNA isolated from female macaques; that is, none of the target-specific primers and probes amplified nontarget sequences (data not shown).

Standard curves were generated successfully from serially diluted pGEMT/*SRY* and pGEMT/DYS14 (Figure 1). We obtained good correlation ($r^2 = 0.97$ and $r^2 = 0.99$, respectively) between C_t values and initial DNA quantities in terms of fold change, with a range of 2×10^1 to 2×10^5 copies per reaction for a subset of *SRY* and DYS14 reactions. PCR amplification efficiencies for *SRY* and DYS14 were 104.6% and 98.6%, respectively. The male-specific gene and sequence were amplified from as few as 20 copies of pGEMT/*SRY* and pGEMT/DYS14 standard plasmid DNA per 25-μL reaction. The lower limit of detection in this 2-color multiplex assay was 20 copies per reaction, whereas little or no amplification resulted from 1 to 10 copies per reaction (Figure 1).

Detection of cell-free fetal DNA in maternal serum. For the detection of cell-free fetal DNA, DNA from the serum of 46 pregnant monkeys was tested by PCR at 5, 12, and 22 wk of gestation. PCR tests for the detection of *SRY* and DYS14 were performed in 11 pregnant monkeys at the fifth week of gestation, 15 at 12 wk, and 15 at 22 wk. We detected both the male-specific *SRY* and DYS14 sequences from cell-free DNA in 28 pregnant monkeys and thus predicted them to have male-bearing pregnancies (Table 2). We predicted that the rest of the pregnancies ($n = 18$) had female fetuses because there was no amplification of the target Y chromosome sequences from the maternal circulation. At all gestational stages, prediction of fetal sex from results of the real-time PCR assay was in 100% accordance with fetal sex determination at the time of delivery. In addition, 100% of the male-bearing pregnant monkeys had detectable levels of cell-free DNA specific for a male fetus.

Absolute quantification of fetal DNA in maternal serum. Quantification data for the copy number of the *SRY* gene and DYS14 sequences during pregnancy are summarized in Table 2. Isolation of DNA from 400 μL of serum consistently produced amplification of the target sequences at 5, 12, and 22 wk of pregnancy in all monkeys bearing a male fetus. The lowest amount of DNA detected in the extracted specimen was estimated to contain 1.0×10^1 DNA copies per 40 μL of the original sample. The average copy number of male fetal DNA with the *SRY* gene in the serum increased significantly at each subsequent pregnancy stage: 75.3,

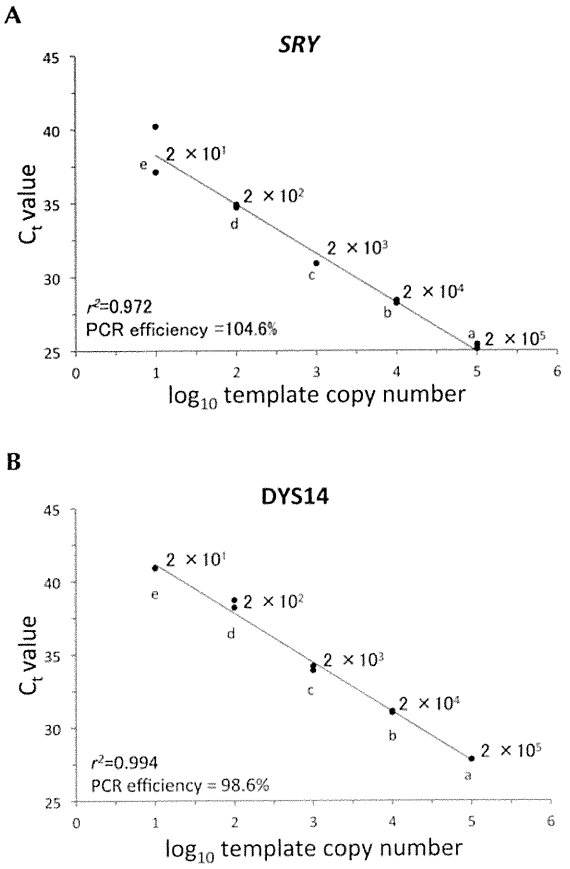

Figure 1. Standard curve and detection limits of copy number for quantification of the *SRY* gene and DYS14 sequences in the *Taq*Man multiplex PCR assay. Data represent the C_t values of 2 repetitions per test. The linear regression line was obtained by plotting the C_t values against the $\log_{10}$ of the initial quantity of the input plasmid DNA. C_t values for both markers were detected at the following template copies per reaction: 2×10^5 (a), 2×10^4 (b), 2×10^3 (c), 2×10^2 (d), and 2×10^1 (e). No C_t value was detected at 2×10^0 template copies per reaction. (A) *SRY* gene. (B) DYS14.

1370.6, and 4705.7 copies per milliliter serum at 5, 12, and 22 wk, respectively ($P < 0.001$ between 5 and 12 wk; $P < 0.05$ between 12 and 22 wk; Table 2). A higher average copy number of DYS14 was detected in the same serum sample as that for *SRY*: 1997.5, 22,718.5, and 54,814.3 copies per milliliter serum ($P < 0.005$ between 5 and 12 wk; no difference between 12 and 22 wk; Table 2).

Comparison of the mean copy numbers of *SRY* and DYS14 at different pregnancy stages in individual monkeys. The analysis for copy number variations of the *SRY* gene and DYS14 sequence were confirmed by the results in 3 of the 5 monkeys tested (nos. 1310107066, 1219302022, 1310006041, 1219408142, and 1219505076) throughout pregnancy (Figure 2) Maternal serum from 1310107066, 1219302022, and 1310006041 contained male-specific DNA detected by PCR, with male fetal sex confirmed at birth; the other 2 monkeys (1219408142 and 1219505076) both carried female fetuses (Table 2). Although interindividual variation in copy number was high for both *SRY* and DYS14 (Table 2 and Figure 2), *SRY* data differed significantly ($P < 0.001$) between the 3 male compared with 2 female offspring (Table 2 and Figure 2). Because of high interindividual variation, average DYS14 copy number in all randomly selected monkeys did not differ between 12 and 22 weeks of gestation, however this parameter did differ ($P < 0.001$) among the subset of monkeys that was monitored throughout pregnancy (Table 2 and Figure 2).

Discussion

The successful detection and quantification of *SRY* and DYS14 sequences in the maternal serum of pregnant cynomolgus monkeys revealed the presence of cell-free fetal DNA in sufficiently high quantities to support analysis. Therefore, the selected primers and probe combinations were effective in differentiating male from female fetal DNA and in detecting male-specific DNA in a laboratory setting.

Our results support the hypothesis that cell-free fetal DNA is reliable for predicting the sex of the fetus at 5, 12, and 22 wk of pregnancy in cynomolgus monkeys. The results obtained from the PCR test using DNA from maternal serum were 100% consistent with observations of the newborns after delivery. We evaluated 2 loci of the Y chromosome, and we were able to demonstrate 100% test specificity and 92% to 100% PCR amplification efficiency for fetal DNA in maternal serum and to determine fetal sex reliably at as early as the fifth week of gestation. Despite disagreement regarding the reliability and diagnostic accuracy of sex determined by fetal DNA in humans at an early stage of pregnancy, cell-free fetal DNA has been detected in nonhuman primates at 20 to 50 d of gestation.[9,10,17] Regardless, we should repeat PCR tests used to detect fetal DNA at an early stage of pregnancy. Using a larger volume of plasma or serum and a highly sensitive molecular technique like our real-time or digital PCR system might help to minimize difficulties in determining fetal DNA in early pregnancy.

Real-time PCR analysis is a highly sensitive method for quantifying genomic DNA. The male-specific *SRY* and DYS14 sequences have been used effectively to track prenatal DNA in human maternal serum samples by using PCR assays.[3,23] The presence of fetal DNA in maternal serum or plasma has been described previously in humans and other species.[7,9] In the current study, we quantified the male-specific genomic cell-free DNA from maternal serum and obtained results that are consistent with others' observations.[9,13] We found a higher copy number of *SRY* in cell-free DNA than did a previous study.[9] The reason might be the sampling stage, because the previous study used a range of gestational days; in contrast, we focused specifically on the gestational time points of weeks 5, 12, and 22. In addition, the DNA extraction method might play a role in the number of copies of cell-free DNA that can be detected. Similar to findings from other studies and by using *SRY* and DYS14 as markers, we confirmed significantly increasing numbers of copies of fetal DNA as pregnancy advanced, suggesting the increased release of placental trophoblast-derived apoptotic bodies to the maternal circulation as the fetus and placenta develop.[3,6]

The number of copies of the DYS14 sequences that we detected was higher than that of the *SRY* gene in the genome. This finding might be due to the presence of a multicopy DYS14 locus in the genome of monkeys, the number of which varies between subjects.[7] Interindividual variation in the copy number of DYS14 has not yet been determined in nonhuman primates, and further detail studies are necessary. The lack of information and incomplete sequence data for the Y-specific